The *glp-1* 3' untranslated region regulates germline proliferation and promotes reproductive fecundity through multiple mechanisms

Peren Coskun and **Sean P. Ryder***

Department of Biochemistry and Molecular Biotechnology, University of Massachusetts Chan Medical School, Worcester, MA, USA

*Corresponding author:

Sean.Ryder@umassmed.edu; 364 Plantation Street LRB-906, Worcester, MA, 01605, USA; 508-856-1372

Keywords: RNA-binding protein, post-transcriptional regulation, nematode, germline, reproduction, fertilization

ABSTRACT

Germline development and successful embryogenesis depend upon the post-transcriptional regulation of maternal mRNAs. In *Caenorhabditis elegans*, the Notch-like receptor *glp-1* is necessary for germline progenitor cell proliferation in adults and anterior cell fate determination in embryos. The spatiotemporal patterning of GLP-1 protein has long served as a paradigm of maternal mRNA regulation in metazoans. The *glp-1* 3'UTR has been shown to be sufficient to pattern the expression of reporter genes, and multiple regulatory regions and RNA-binding protein interaction sites have been mapped. The RNA-binding proteins POS-1 and GLD-1 directly regulate *glp-1* mRNA via sequence specific interactions with motifs found in the *glp-1* 3'UTR. The impact of mutating the endogenous *glp-1* 3'UTR has not been studied, and the mechanism by which POS-1 and GLD-1 mediate repression is not understood. Here, we investigate the post-transcriptional mechanisms that govern *glp-1* expression, revealing that GLD-1 and POS-1 regulate this pattern through different pathways requiring different co-factors. Remarkably, mutations in the endogenous locus that disrupt either POS-1 or GLD-1 binding to the *glp-1* 3'UTR have minimal impact on reproductive fecundity. By contrast, a larger deletion that eliminates the binding of both has a strong effect on brood size, hatch rate, and displays an increase in the length of the germline mitotic region that corresponds with enhanced mitotic activity. Together, our results show that multiple post-transcriptional mechanisms work in concert to ensure robust GLP-1 patterning and thus maximize reproductive outcomes.

INTRODUCTION

Female gametes are larger than their male counterparts and provide most of the cytoplasm to a newly fertilized zygote. The cytoplasm is loaded with mRNAs, proteins, and nutrients that are necessary for the zygote to progress through several rounds of cell division. In most species, early developmental decisions such as axis polarization, germline / soma segregation, and initial cell fate patterning decisions occur prior to zygotic gene activation (ZGA)—the point where zygotic transcription begins and the maternal mRNA supply is turned over [1]. As such, post-transcriptional regulatory mechanisms are thought to be crucial to regulating maternal mRNAs, ensuring that key cell fate specifying proteins are produced at the right place and time, thus enabling successful embryogenesis [2-6]. In the nematode model organism *Caenorhabditis elegans*, zygotic transcription begins at the four-cell stage in somatic lineages and after the >100 cell stage in the germline lineage [7-9]. Accordingly, several maternally supplied mRNAs have been shown to be important for early developmental decisions [10-14]. Mutations in these genes are often maternal effect lethal or maternal effect sterile [15].

In worms, the 3'UTR is the primary region that governs maternal RNA regulation in the germline [16]. Many *C. elegans* mRNAs go through a *trans* splicing reaction to add the 5' cap structure, substituting the endogenous 5' end of the transcript with one of two splice leader sequences [17]. As such, many transcripts are identical at the 5' end. Reporter transgenes that fused the 3'UTRs of several germline transcripts to a fluorescence reporter gene and a generic germline promoter shows that the 3'UTR match the pattern of the endogenous gene in nearly all cases [16]. The sole exceptions were sperm-specific genes, whose patterning is governed by their promoters [16]. In a seminal discovery, the 3'UTR of *glp-1* mRNA was shown to be sufficient for the spatiotemporal patterning of a series of injected mRNA reporters, demonstrating patterning sufficiency in the absence of transcription, and revealing the post-transcriptional basis for GLP-1 regulation [4].

59 The *glp-1* gene encodes a Notch protein that receives cell signaling cues to activate pro-
60 mitotic transcriptional programs in the distal end of the germline [18]. In germline progenitor cells,
61 GLP-1 receives a signal from the Delta-like ligand LAG-2, expressed on the somatic distal tip cell
62 [19]. This interaction drives a conformational change in GLP-1 that promotes site-specific cleav-
63 age inside germline progenitor cells, releasing a C-terminal domain that enters the nucleus to
64 promote transcription of mitotic genes, thus enabling germline progenitor cell renewal [20]. GLP-
65 1 also promotes anterior cell fate specification in the embryo by transmitting signals between
66 anterior and posterior blastomeres [18, 21]. GLP-1 is expressed in anterior lineage cells of early
67 embryos, where it receives a signal from a second Delta-like ligand APX-1 to promote pharyngeal
68 cell fate specification [5, 22, 23]. As such, the precise spatial patterning of GLP-1 is essential to
69 both germline proliferation and anterior development in embryos. Accordingly, a loss of function
70 *glp-1* mutant depletes progenitor cells rapidly and becomes sterile [18]. Embryos produced from
71 *glp-1* mutant mothers fail to form the pharynx and arrest during morphogenesis [18, 22].
72 Transcripts encoding *glp-1* are observed throughout the germline and in all cells of the
73 early embryo. By contrast, GLP-1 protein expression is restricted to the mitotic zone in the
74 germline and the anterior cells of early embryos [4, 24]. The expression pattern is reported to be
75 controlled by several RNA-binding proteins including MEX-3, OMA-1, PUF-3, PUF-5/6/7, GLD-1,
76 POS-1 and SPN-4 (**Fig. 1A, B**) [25-30]. In the germline, GLD-1 represses GLP-1 expression in
77 the meiotic zone [29], while OMA-1/2, PUF-3, MEX-3, and PUF-5/6/7 repress expression in oo-
78 cytes [26, 27, 31]. In the embryos, GLD-1 and POS-1 repress GLP-1 expression in early posterior
79 lineage cells [29]; and MEX-5/6 and SPN-4 promote GLP-1 expression in early anterior lineage
80 cells [30].

81 Precise mutational studies of the *glp-1* 3'UTR in the context of injected mRNAs or trans-
82 genic reporters identified specific regions and precise binding motifs that are necessary for *glp-1*
83 regulation (**Fig. 1C**) [4, 29, 32]. GLD-1 and POS-1, two key repressors of GLP-1 translation,

recognize partially overlapping motifs within a region of the *glp-1* 3'UTR that governs its spatial control [29, 32]. GLD-1, a STAR/GSG/Maxi-KH domain RBP, binds to UACUC/AAY motifs (GLD-1 binding motif: GBM) [33-36], whereas POS-1—a CCCH type zinc finger protein—recognizes UAUUA/G(A/G/U)NNG motifs (POS-1 recognition element: PRE) [12, 37]. The motifs for both RBPs are present in a previously mapped *glp-1* repression element (GRE) [29]. A second POS-1 binding motif is positioned in the adjacent *glp-1* derepression element (GDE), a region previously shown to be necessary for reporter expression [29]. The physical interaction of each RBP to their respective element has confirmed in vitro. The GLD-1 binding site partially overlaps with both POS motifs, and *in vitro* binding studies showed the two RBPs compete for binding to this region of the *glp-1* 3'UTR [32].

Mutagenesis studies identified specific separation of function mutations that disrupt each binding site without perturbing binding to the other adjacent sites [32]. In transgenic reporter studies, the GLD-1 motif in the GRE and the POS-1 motif in the GDE were both required for repression in the posterior of embryos [32]. By contrast, the 5' POS-1 motif appears to be non-functional in the reporter [32]. Mutation of the GLD-1 motif led to elevated expression in the meiotic zone of the adult germline, while mutation of the POS-1 motif led to reduced expression in the same region [32]. Although the *glp-1* 3'UTR has been studied for over three decades [4], there have been no mutational studies conducted at the endogenous locus, and the biological significance of the *glp-1* 3'UTR to the worm reproduction has yet to be characterized.

In this study, we combine genetic and molecular approaches to assess the mechanism of *glp-1* mRNA regulation and its biological impact on reproduction, focusing on the well-characterized GLD-1 and POS-1 binding elements. Our data reveal that GLD-1 and POS-1 repress *glp-1* through shortening of the polyA tail; however, our data also show that they appear to work via different pathways requiring different co-factors. Moreover, our work shows that translational control of *glp-1* by the cap-binding factor *ife-3* is important for repression in the germline, but neither

109 the POS-1 nor GLD-1 binding sites contribute to this repression. Finally, our work shows that
110 mutation of the POS-1 or GLD-1 binding sites in the endogenous *glp-1* 3'UTR has limited impact
111 on reproductive fecundity in isolation, but deleting a region containing both sites has a strong
112 reproductive phenotype—impacting fecundity, embryonic viability, and gene expression patterns.

113

114 **RESULTS**

115 *The glp-1 3'UTR isoform distribution and polyA tail length are not impacted by loss of pos-1, gld-*
116 *2, gld-3, mex-5, or mex-6 in embryos*

117 The *glp-1* 3'UTR is necessary and sufficient to confer the GLP-1 expression pattern to a
118 reporter transgene [4, 16, 32]. We set out to understand how this 3'UTR governs this pattern of
119 expression. Transcripts can have different 3'UTRs as the consequence of alternative splicing (AS)
120 or alternative polyadenylation (APA) [38]. Two separate studies mapped all *C. elegans* 3'UTRs
121 using RNA collected from worms ranging in age from embryos to young adults [39, 40]. From
122 these data, the *glp-1* 3'UTR was shown to have six possible isoforms that appear to derive from
123 solely from APA. The UTR isoforms (A-F) range from 102 to 411 nucleotides in length (**Fig. 2A**).
124 Isoforms A and B lack the previously mapped GRE and GDE elements, including the GLD-1 and
125 POS-1 binding sites, but isoforms C to F do contain these motifs.

126 To evaluate the distribution of *glp-1* 3'UTR isoforms in embryo samples, we analyzed
127 reads corresponding to each isoform variant from published polyA-test sequencing (PAT-seq)
128 data [41]. This data set contains samples obtained from N2 embryos, samples collected from
129 embryos with *pos-1*, *gld-2*, *gld-3*, or *mex-5* RNAi treatment, as well as samples recovered from
130 *mex-5(pk440)* mutant embryos. To recover reads mapping to the *glp-1* gene from each data set,
131 raw sequencing data were downloaded from the NCBI sequence read archive corresponding to
132 Bioproject PRJNA248658. The raw data were analyzed with custom scripts (see methods) con-
133 taining a pattern matching algorithm to recover reads harboring each of the possible *glp-1* UTR

134 isoforms, as well as the corresponding polyA tail length. The data show that only isoform D is
135 present in embryo samples recovered from all genotypes and treatment conditions. The median
136 polyA tail length is 18 adenosines for all samples except *mex-5* RNAi, where the median tail length
137 is 20 adenosines (**Fig. 2B**). There is no statistically significant difference in the mean polyA tail
138 length in all six samples (p_{adj} ~ 1.0, **Supplemental Data Set 1**). The data do show that *glp-1* polyA
139 tails in embryos are considerably shorter than the median polyA length in *C. elegans* (57 nucleo-
140 tides) [42]. They are shorter than what is believed to be the minimal length necessary to support
141 efficient translation (20 nucleotides) [42]. RNAi knockdown or mutation of five different RNA-bind-
142 ing proteins, including *pos-1*, does not appear to impact the median length or the isoform distri-
143 bution in embryos.

144

145 *The glp-1 3'UTR polyA tail length is shorter in embryos than in young adults*

146 To determine how polyA tail length is impacted by POS-1 and GLD-1 binding site muta-
147 tions in the *glp-1* 3'UTR, we measured the polyA tail length distribution in our previously described
148 *glp-1* 3'UTR reporter transgenes [37] (**Fig. 2C-D**). The advantage of measuring the distribution in
149 the transgenic reporters is that RNAi of *pos-1*, *gld-2*, and *gld-3* is known to induce strong pheno-
150 types in the germline or embryo [12, 43, 44]. These phenotypes could have indirect effects on the
151 polyA tail length. The disadvantage is that endogenous *glp-1* transcripts are also present in these
152 strains, which necessitates an assay that distinguishes reporter mRNAs from endogenous *glp-1*
153 transcripts. Total RNA was recovered from adults and/or embryos from the WT *glp-1* 3'UTR re-
154 porter (WRM5: hereafter *glp-1* WT, **Table 1**), the GLD-1 binding motif mutant 3'UTR reporter
155 (WRM6: hereafter *glp-1* GBM), or a reporter where both POS-1 binding sites are mutated (WRM9:
156 hereafter *glp-1* 5'3'PRE) [37]. Recovered transcripts were tailed with guanosine and inosine using
157 established protocols [45] and then amplified using RT-PCR with a 5'-polyC-TT-3' tail primer and
158 a forward primer that anneals to the GFP reporter, preventing endogenous transcript amplification

159 (**Fig. 2C**). The amplicon was topo-cloned, transformed into *Escherichia coli*, and multiple individ-
160 ual colonies were sequenced for each sample using Sanger sequencing to estimate the isoform
161 ratio and length of the polyA tails (**Fig. 2D**).

162 Consistent with the genome-wide data, we only observe transcripts corresponding to iso-
163 form D. Our results show that the median polyA tail length is 29 in young adult *glp-1* WT animals,
164 27 in *glp-1* GBM, and 31 in *glp-1* 5'3'PRE. The data demonstrates that mutation of the GLD-1 and
165 POS-1 binding sites do not alter the polyA tail distribution in young adults (p_{adj} = 1.00, **Fig. 2D**). In
166 embryo samples collected with the reporter transgenes, the polyA tail length is considerably
167 shorter in *glp-1* WT embryos compared to young adults (*glp-1* WT_{YA} = 29, *glp-1* WT_{emb} = 12, p_{adj}
168 = 3.8e-4, **Fig. 2D**), suggesting that polyA tail lengths are shortened between the adult germline
169 and fertilized embryos. This observation is consistent with the genome wide study that showed
170 short polyA tails on endogenous *glp-1* transcripts (**Fig 2B**)**.** PolyA tail shortening is not observed
171 in *glp-1* GBM or *glp-1* 5'3'PRE reporters (*glp-1* GBM_{YA} =27, *glp-1* GBM_{emb} = 29, p_{adj} = 1; *glp-1*
172 5'3'PRE $_{YA}$ = 31, *glp-1* 5'3'PRE $_{emb}$ = 42, **Fig. 2D**). Together, the results suggest that derepression
173 of the *glp-1* GBM and *glp-1* 5'3'PRE reporter transgenes in embryos is caused in part by failure
174 of a polyA tail shortening mechanism that acts on the wild-type 3'UTR.

175

176 *GLD-2 and GLD-4 cytoPAPs contribute to glp-1 polyA tail distribution in different ways*

177 We were intrigued by the difference in embryonic polyA-tail distribution in the *glp-1* GBM
178 and/or *glp-1* 5'3'PRE reporter transgenes and wondered if cytoplasmic polyA polymerase activity
179 contributes to derepression. GLD-2 and GLD-4 are both well-characterized cytoplasmic polyA
180 polymerases found in early embryos [44, 46, 47]. We knocked *gld-2* or *gld-4* down using RNAi in
181 all three reporter strains and quantified the GFP fluorescence intensity in each cell of dissected
182 four-cell embryos, comparing the pattern and intensity of the fluorescence (**Fig. 3A**). In untreated

183 *glp-1* WT embryos, reporter expression is biased towards anterior cells, as previously reported
184 [32]. In untreated *glp-1* GBM and *glp-1* 5'3'PRE mutant embryos, expression is increased and
185 observed in all four cells (Fold Effect *glp-1* GBM / *glp-1* WT = 3.0; p_{adj} = <1e-12; *glp-1* 5'3'PRE /
186 *glp-1* WT = 3.4, p_{adj} = <1e-12, **Fig. 3A,B**) [32]. RNAi of *gld-2* or *gld-4* had no significant impact on
187 the abundance or pattern of GFP fluorescence in *glp-1* WT UTR embryos (*glp-1* WT_{gld-2} / *glp-1*
188 WT_{ctl} = 1.0; p_{adj} = 1.0; *glp-1* WT_{gld-4} / *glp-1* WT_{ctl} = 1.4, p_{adj} = 1.0; **Fig. 3C**). However, *gld-2* RNAi
189 caused a decrease in the fluorescence intensity of both the *glp-1* GBM and *glp-1* 5'3'PRE report-
190 ers (*glp-1* GBM_{gld-2} / *glp-1* GBM_{ctl} = 0.73, p_{adj} = 0.00026; *glp-1* 5'3'PRE_{gld-2} / *glp-1* 5'3'$PRE_{control}$ =
191 0.72, p_{adj} = 6.47e-7; **Fig. 3D,E**). This suggests that GLD-2 contributes to the derepression that is
192 observed when either the GLD-1 or POS-1 binding sites are mutated. Intriguingly, in *gld-4* RNAi
193 animals, different results were observed in the GBM versus 5'3'PRE reporters, with total fluores-
194 cence increasing in *glp-1* GBM but remaining unchanged in the 5'3'PRE reporter (*glp-1* GBM_{gld-4}
195 / *glp-1* GBM_{ctl} = 1.36, p_{adj} = 1.7e-7; *glp-1* 5'3'PRE_{gld-4} / *glp-1* 5'3'PRE_{ctl} = 1.05, p_{adj} = 1.0; **Fig. 3D,E**).
196 These results show that knock down of *gld-2* and *gld-4* have opposing effects on the *glp-1* GBM
197 reporter, and that knock down of *gld-2*, but not *gld-4*, impacts the expression from the *glp-1*
198 5'3'PRE reporter.

199

200 *Regulation of glp-1 3'UTR reporter transgenes by ife-3*

201 We are also interested in understanding *glp-1* 3'UTR reporter transgene regulation in the
202 germline. Several key regulatory factors, including translation initiation factors, cause sterility or
203 embryonic lethality when mutated. As such, we chose to investigate their impacts on the *glp-1*
204 3'UTR reporter variants in oocytes. We chose three germline expressed eIF4E-binding proteins
205 homologs (*ife-1*, *ife-2*, and *ife-3*) for RNAi knockdown. We measured the mean GFP intensity of
206 the four most proximal oocytes in all three reporter strains treated with RNAi targeting each of
207 these ten regulatory factors compared to controls. We observe no change in the mean

208 fluorescence intensity of worms treated with *ife-1* or *ife-2* in any of the three strains (**Fig. 3F,G**,
209 **Supplemental Data Set 1**). However, we observe a strong upregulation of all three reporters
210 upon *ife-3* knockdown (Fold Effect *glp-1* WT_{ife-3} / *glp-1* WT_{ctl} = 1.37, p_{adj} = 1.05e-9; Fold Effect *glp-*
211 *1* GBM_{ife-3} / *glp-1* GBM_{ctl} = 1.48, p_{adj} = 2.89e-8; Fold Effect *glp-1* 5'3'PRE_{ife-3} / *glp-1* 5'3'PRE_{ctl} =
212 2.05, p_{adj} = <1e-7). Taken together, the data suggest that GLD-2 activates transgene expression
213 in embryos, but only under derepressed conditions (**Fig. 3H**). In contrast, GLD-4 represses
214 transgene expression in embryos, potentially via the POS-1 binding site. IFE-3 represses
215 transgene expression in oocytes, but this mechanism seems to be independent of the POS-1 or
216 GLD-1 binding sites.

217

218 *Mutation of the GLD-1 and POS-1 binding sites in the endogenous glp-1 gene*

219 To understand the physiological impacts of mutating the GLD-1 and POS-1 binding sites in the
220 endogenous *glp-1* locus, we used CRISPR-Cas9 mutagenesis to make precise mutations in an
221 OLLAS-tagged *glp-1* strain corresponding to the variants we previously made in our reporter
222 strains (**Fig. 4A**) [32, 48]. Our design also includes removal of a protospacer adjacent motif (PAM)
223 to prevent re-cleavage of the knock in mutation, and mutation of a HindIII restriction site to facili-
224 tate screening. In total, we produced three strains: *glp-1(spr21[q977*])*, a control strain with the
225 PAM site deletion and the HindIII site insertion that is otherwise wild-type (WRM83: hereafter *glp-*
226 *1(WT*)*); *glp-1(spr33[q977*])* which is identical to *glp-1(WT*)* except it also harbors the GBM mu-
227 tation (WRM109: hereafter *glp-1(GBM)*); and *(glp-1(spr22[q977*])* which harbors the 5'3'PRE mu-
228 tation (WRM84: hereafter *glp-1(5'3'PRE)*, **Table 1**). All three strains can be easily propagated as
229 homozygotes.

230 To determine whether the GBM and 5'3'PRE mutations affect reproductive fecundity, we
231 measured the total brood size and hatch rate for all three strains. Under standard growth

232 conditions at 20°C, the brood size and hatch rate are nearly identical for *glp-1 (WT*)*, *glp-1(GBM)*,
233 and *glp-1 (5'3'PRE)* alleles (**Fig. 4B,C**, **Supplementary Data Set 1**). Because 3'UTR mutations
234 in other maternal transcripts have shown enhanced phenotypes at elevated temperatures [49,
235 50], we repeated the measurements with worms grown at 25°C. Under these conditions, the total
236 brood size is similar in all three strains, but the hatch rate was mildly reduced in *glp-1(5'3'PRE)*
237 compared to the *glp-1(WT*)* allele (Fold effect: *glp-1(5'3'PRE)* / *glp-1(WT*)* = 0.96, padj = 0.001,
238 **Fig. 4B,C**). The hatch rate in *glp-1(GBM)* is unaffected. The results show that mutations that
239 cause strong derepression of a *glp-1* reporter in embryos do not cause strong reproductive phe-
240 notypes when engineered into the endogenous locus, suggesting that reproduction is robust to
241 dysregulation mediated by loss of either POS-1 or GLD-1 binding sites.

242

243 *Mutation of a region including both GLD-1 and POS-1 sites reduces fertility*

244 Next, we used CRISPR to make a deletion of the *glp-1* 3'UTR (*glp-1(spr16[*q977])*) that
245 removes both POS-1 binding sites, the GLD-1 binding site, and adjacent sites predicted to be
246 recognized by FBF-1/2 and/or MEX-3. In total, this deletion precisely removes 71 base pairs from
247 the 3'UTR (hereafter *glp-1(Δ71)*, **Fig. 4A**). In designing this deletion, we were able to identify a
248 guide RNA that recognizes the region to be deleted in our intended mutation, obviating the need
249 for the PAM deletion and HindIII site insertion used in making the precise binding site alleles
250 described above. Despite deleting a region of the 3'UTR that has been shown to be sufficient for
251 spatial patterning of a reporter [4], *glp-1(Δ71)* is viable and easily propagated as a homozygote.
252 To assess the impact of this mutant on worm reproduction, we conducted brood size assays at
253 both 20°C and 25°C. At 20°C, we observed a 1.7-fold reduction in the mean brood size of *glp-*
254 *1(Δ71)* compared to the parent strain (*glp-1(q977)*), hereafter *glp-1(WT)*, p_{adj} = <1e-10, **Fig. 4B**).
255 We also observed a 2.5-fold decrease in the hatch rate of *glp-1(Δ71)* embryos compared to the
256 background strain (p_{adj} = <1e-10, **Fig. 4C**). In parallel to our findings at 20°C, we observed reduced

257 brood size and hatch rate at 25°C for *glp-1(Δ71)* compared to the control (Fold effect reduction in
258 total brood = 1.2, p_{adj} = 0.00003; Fold effect reduction in hatch rate = 1.35, p_{adj} = <1e-10, **Fig.**
259 **4B,C**). The difference in magnitude could be caused by the reduction of the brood size in the
260 control *glp-1(WT)* strain at elevated temperature as opposed to temperature-dependent rescue in
261 the mutant. The results show that the *glp-1* 3'UTR region containing the GLD-1, POS-1, and ad-
262 jacent RBP-binding sites contributes to the total fecundity and successful embryogenesis, both
263 under standard growth conditions and at elevated temperature.

264

265 *The Δ71 glp-1 3'UTR mutation produces terminal embryos that are distinct from a loss-of-function*
266 *allele*

267 On average, when incubated at 20ºC, more than 60% of *glp-1(Δ71)* embryos fail to hatch.
268 Loss-of-function *glp-1* mutants also produce embryos that fail to hatch, but with complete pene-
269 trance. We sought to compare the *glp-1(Δ71)* phenotype to the loss-of-function phenotype. We
270 used DIC microscopy to image embryos harvested from *glp-1(WT)*, *glp-1(Δ71)*, and *glp-1(or178)*,
271 which encodes a strong temperature sensitive loss-of-function allele (hereafter *glp-1(ts)*). Embryo
272 images were binned by developmental stage and annotated based upon their appearance as
273 normal or abnormal (**Fig. 5**). All early-stage embryos (one cell to 64-cell) produced by *glp-1(WT)*
274 and *glp-1(ts)* looked normal in appearance (n=41, n=27, **Fig. 5A-C**). By contrast, 33% of *glp-*
275 *1(Δ71)* early embryos appeared defective (n=9/27, p_{adj} = 1.4e-4, **Fig. 5B**). In later stage embryos
276 (65-cell to pretzel stage), 90% of embryos were normal in *glp-1(ollas)* (n=26/29), while just 61%
277 of *glp-1 (Δ71)* (n=64/105, p_{adj} = 0.007) and 52% of *glp-1(ts)* embryos (11/21, p_{adj} = 0.006) ap-
278 peared normal (**Fig. 5D-F**). Most of the terminal *glp-1(ts)* embryos resembled the published *glp-*
279 *1* loss-of-function phenotype with arrest after morphogenesis begins (**Fig. 5F**) [18]. In contrast,
280 the *glp-1(Δ71)* embryos appeared to show a more variable phenotype, including regions of bun-
281 dled cells and zones of clearing presumably due to apoptosis (**Fig. 5B,E**). These defects appear

282 to manifest after the 16-cell stage but before morphogenesis. A quantitation of these results is
283 shown in **figure 5G**. Together, our results suggest that the cause for embryonic lethality in *glp-*
284 *1(Δ71)* embryos is distinct from loss of function *glp-1* alleles.

285

286 *Increased germline mitosis in glp-1(Δ71) mutants*

287 In the germline, GLP-1 protein expression is restricted to the distal end [24], and the re-
288 pression of *glp-1* translation by the RNA-binding protein GLD-1 is thought to promote meiosis
289 [29]. Consistent with this model, a gain-of-function *glp-1* allele forms a germline progenitor cell
290 tumor [51], phenocopying strong loss-of-function *gld-1* alleles [10]. To evaluate the impact of the
291 3'UTR deletion on GLP-1 expression pattern in the germline, we dissected gonads from *glp-*
292 *1(WT)* and *glp-1(Δ71)* young adult hermaphrodites, fixed them, and stained for the OLLAS tag
293 on *glp-1*. We also imaged with DAPI to assess the morphology of the nuclei and determine the
294 length of the mitotic zone (**Fig. 6A-F**). OLLAS immunofluorescence reveals that GLP-1 protein
295 is expressed in both wildtype and Δ71 mutants in the distal arm of the germline to approximately
296 the same level (**Fig. 6A**, **D**). To quantify the pattern of GLP-1 expression, we measured the dis-
297 tance from the distal tip of the gonad to the end of the OLLAS positive region in both *glp-1(WT)*
298 and *glp-1(Δ71)* embryos. In gonads dissected from control animals, the average length of the
299 OLLAS positive region is 113.2 ± 25 microns. In mutants, the length increases to 117.9 ± 20.7
300 microns, suggesting that GLP-1 expression is not expanded proximally in the Δ71 3'UTR dele-
301 tion ($p = 0.47$, **Fig. 6G**).

302 GLP-1 promotes mitotic gene expression in the distal end of the germline [18, 24]. To as-
303 sess whether mitosis is increased in the 3'UTR mutant, we counted the number of distal mitotic
304 figures present in the DAPI channel of the OLLAS immunofluorescence images described
305 above. We also measured the overall length of the mitotic zone, defined as the distance from

306 the distal end of the germline to the first crescent-shaped meiotic nucleus [52]. We observe an
307 increase in the average number of mitotic figures in Δ71 mutants compared to controls (Δ71 =
308 3.69 ± 2.37, n = 26; control = 1.73 ± 0.77, n = 26; p = 0.00021, **Fig. 6H**). This corresponds to an
309 increase in the average length of the mitotic zone in mutants (Δ71 = 131.2 ± 20, n = 26; control
310 = 80.5 ± 23.2, n = 26; p = 3.7e-11, **Fig. 6G**). As an independent measure of increased mitosis,
311 we stained for PH-3 positive nuclei in in the distal end (**Fig. 6I-L**). We observe twice as many
312 PH-3 positive nuclei in the *glp-1(Δ71)* mutant compared to control (Mean PH-3+ (Δ71) = 6.4 ± 2,
313 n = 34; PH-3+ (control) = 3.2 ± 2, n = 36, p = 6.6e-8, **Fig. 6M**). Together, the data show that the
314 pattern of GLP-1 expression is enlarged in the Δ71 mutant, and this increase correlates to an
315 increase in the number of germline progenitor cells undergoing mitosis.

316

317 *Mutation of the glp-1 3'UTR leads to changes in stress response and metabolism gene expression*

318 To understand how dysregulation of *glp-1* expression in *glp-1(Δ71)* mutants impacts gene
319 expression, we performed RNA-seq on age matched young adult hermaphrodites from synchro-
320 nized populations of *glp-1(ollas)* and *glp-1(Δ71)* mutants. We also collected samples from syn-
321 chronized young adult *glp-1(WT)*, *glp-1(GBM)*, and *glp-1(5'3'PRE)* animals. Data were analyzed
322 with the OneStopRNASeq pipeline [53], and gene expression differences between genotypes
323 were assessed using DESeq2 with a $\log_2$ fold change cutoff of ≤ ±0.585 and a p_{adj} cutoff of ≤ 0.05
324 (**Fig. 7A-C**) [54]. The full analyses are available in **Supplemental Data Set 2**. Comparing *glp-*
325 *1(ollas)* to *glp-1(Δ71)*, we observe 81 upregulated and 405 downregulated genes. Comparing *glp-*
326 *1(WT)* to *glp-1(GBM)* and *glp-1(5'3'PRE)* mutants, we see far fewer gene expression changes.
327 We observe seven upregulated and one downregulated in *glp-1(GBM)*, and nine upregulated with
328 six downregulated in *glp-1(5'3'PRE).* Five of the 81 upregulated genes in *glp-1(Δ71)* are also
329 upregulated in the *glp-1(GBM)* or *glp-1(5'3'PRE)* mutants (**Fig. 7D**). Just one of the 405 downreg-
330 ulated genes in *glp-1(Δ71)* is shared with another mutant of the *glp-1* 3'UTR (5'3'PRE, **Fig. 7E**).

331 The data show that the number of gene expression changes correlates with the magnitude of the
332 impact on reproductive fecundity, and that most gene expression changes observed in *glp-1(Δ71)*
333 are unique to that mutant. The abundance of *glp-1* mRNA is unchanged in all three mutants,
334 suggesting that *glp-1* mRNA abundance is not impacted by either binding site mutation or by the
335 larger deletion.

336 Focusing on the *glp-1(Δ71)* mutant, we used WormCat 2.0 to determine which gene sets
337 are perturbed in this mutant compared to control (**Fig. 7F, Supplemental Data Set 2**) [55]. The
338 results show that metabolism and stress response genes are overrepresented in the total regu-
339 lated gene set (both up and downregulated genes, p_{adj} = 2.7e-13 (metabolism); p_{adj} = 3.3e-7
340 (stress response)). Specifically impacted metabolic pathways include amino acid metabolism, li-
341 pid metabolism, creatine kinase, and glycolysis. We also observe changes in somatic genes in-
342 volved in neuronal and muscle function, although at a lower frequency (p_{adj} = 7.7e-8 (neuronal);
343 p_{adj} = 1.5e-6 (muscle)). Using tissue enrichment analysis on upregulated genes, we see an en-
344 richment for genes expressed in the germline (Q-value = 0.00014) and oocytes (Q-value = 0.012,
345 **Supplemental Data Set 2**), consistent with ectopic mitosis in the germline [56]. Repeating the
346 tissue enrichment analysis on downregulated genes, we see enrichment of genes expressed in
347 several muscle lineages (MS, D, and C lineage), as well as the head mesodermal cell (MS) and
348 the VC2 and VC3 neurons (P3, P5 lineages, **Supplemental Data Set 2**). The results suggest the
349 possibility of posterior patterning defects in *glp-1(Δ71)* embryos, possibly caused by dysregulation
350 of GLP-1 in the mutant. These changes may account for the observed reduced fecundity in this
351 mutant, but more work will be necessary to understand the precise mechanism.

352

353 **DISCUSSION**

354 The regulation of *glp-1* mRNA has served as a paradigmatic example of post-transcrip-
355 tional control of maternal transcripts for over three decades. A pioneering study demonstrated that

356 the *glp-1* 3'UTR is sufficient to pattern the expression of injected reporter mRNAs [4]. Subsequent
357 work using reporter transgenes confirmed this observation [16], and specific functional elements
358 within the 3'UTR were mapped using both approaches [4, 29, 32]. Here, we expanded upon these
359 foundational studies in two ways. First, we evaluated the mechanism of regulation for two func-
360 tional elements recognized by the RNA-binding proteins GLD-1 and POS-1 across the oocyte-to-
361 embryo transition. Second, we evaluated three alleles corresponding to previously identified func-
362 tional regions of the 3'UTR, defining their importance to reproductive fecundity.

363 Our work suggests that endogenous *glp-1* mRNA undergoes a shortening of the polyA tail
364 as transcripts move from the adult germline to embryos. Loss of the GLD-1 or POS-1 binding
365 motifs (GBM and 5'3'PRE) prevents this shortening, consistent with our prior work that demon-
366 strated an increase in reporter expression in the posterior of the embryo in reporter transgenes
367 [32]. The increase in fluorescence observed in both mutants depends upon the cytoplasmic polyA
368 polymerase GLD-2, suggesting that the mechanism of repression in embryos includes prevention
369 of A-tail lengthening in embryos by this enzyme. Consistent with that model, the average polyA
370 tail length of GBM and 5'3'PRE mutant reporters is longer than WT embryos. Intriguingly, knock
371 down of a second cytoplasmic polyA polymerase, GLD-4, causes the opposite effect. Our findings
372 suggest that GLD-4 plays a repressive role in embryos, working in opposition to GLD-2, but the
373 exact mechanism remains unknown. Knock down of GLD-4 had no impact on the 5'3'PRE, sug-
374 gesting the possibility that GLD-4-dependent repression acts through the POS-1 binding site, ei-
375 ther directly through POS-1 or via an indirect mechanism. Our work also shows that none of the
376 deadenylase enzymes are required for *glp-1* regulation, at least in oocytes, although this obser-
377 vation is limited by the potential for functional overlap between multiple deadenylase enzymes.
378 Lastly, we observe that the atypical eIF4E homology *ife-3* represses all three GLP-1 reporters in
379 oocytes, consistent with models indicating a translational control mechanism in the germline [57].

380 Together, the data shows that multiple mechanisms contribute to *glp-1* repression, and the pre-
381 dominant mechanism changes from oocytes to embryos.

382 Our work also shows that precise mutations in the GLD-1 and POS-1 binding sites do not
383 cause strong reproductive or molecular phenotypes when engineered into the endogenous *glp-1*
384 locus. There are several potential explanations for this apparent dichotomy. First, there could be
385 functional redundancy between the binding sites, although the reporter transgene data support a
386 model where binding of both proteins is needed for full repression. Second, additional mecha-
387 nisms that act on GLP-1 protein, but not on a GFP reporter, may buffer modest changes in GLP-
388 1 expression. Lastly, it is possible that additional binding sites in the coding sequence of *glp-1*
389 mRNA could compensate for loss of the binding sites in the 3'UTR. The finding that a larger de-
390 letion that removes all three motifs confers a much stronger reproductive phenotype supports the
391 first hypothesis.

392 How does dysregulation of *glp-1* lead to embryonic lethality? Our RNA sequencing data
393 provide a few clues. The tissue enrichment analysis reveals that genes from the C, D, and MS
394 lineage muscle tissues are preferentially downregulated in *glp-Δ71* mutant embryos. All three lin-
395 eages are posterior in origin, deriving from cells that normally do not express GLP-1 protein. It is
396 possible that loss of posterior lineage cell specification could account for the changes we observe
397 in these tissues. Similarly, amino acid metabolism and creatine kinase activity is associated with
398 muscle development and activity. The reduction we observe in genes expressed in these path-
399 ways could be explained by reduced development of muscle tissue in embryos. Consistent with
400 this hypothesis, most *glp-1(Δ71)* mutant embryos fail before gastrulation, consistent with cell fate
401 specification defects. We note that the terminal phenotype differs both in the timing of embryonic
402 arrest and in the appearance of the terminal embryos from a *glp-1* null embryos, which fail during
403 morphogenesis with anterior pharyngeal tissue defects [22].

404 Specific metabolism genes that are downregulated in our dataset include *pah-1*, *ceeh-2*
405 and Y51H4A.7. The *pah-1* gene is involved in anabolism [58]. The *ceeh-2* gene is an epoxide
406 hydrolase that functions in lipid signaling [59]. The human UROC1 homolog Y51H4A.7 is thought
407 to operate in histidine degradation [60]. We also note that stress response genes appear to be
408 downregulated in the mutant. Among the downregulated stress response genes are *cdr-2*, *clec-*
409 *48*, and F35E12.6, C49C8.5, and ZK6.11.1. The *cdr-2* gene is involved in the response to cad-
410 mium [61]; whereas F35E12.6, C49C8.5, ZK6.11.1, and *clec-48* genes have reported roles in the
411 innate immune response [62].

412 Conversely, the upregulated gene set is limited to germline and/or oocyte expressed
413 genes that mostly have unassigned functions. The most upregulated gene is C55C3.3, a mem-
414 brane-associated protein of unknown function that appears to be broadly conserved in nematodes
415 in a BLASTP analysis [63]. This gene encodes a prion like (Q/N) domain with 41 glutamines and
416 27 asparagines. The protein also harbors a serine-proline rich region, encoding 57 serines and
417 58 prolines. This transcript is also upregulated in the *glp-1(GBM)* mutant, but not in the *glp-*
418 *1(5'3'PRE)* mutant. Knock down of the C55C3.3 in a *rrf-3* sensitized genome-wide RNAi screen
419 causes embryonic lethality [64]. However, a loss of function allele does not appear to have this
420 phenotype. Additional upregulated genes include *haf-6*, *lin-15A*, *lin-15B* and *tbc-1*. *tbc-1* was re-
421 ported to have functions in innate immunity [65]; *haf-6* is a member of ATP-binding cassette trans-
422 porters and found to be necessary for RNA interference [66]. *lin-15A* and *lin-15B* have functions
423 in vulval development [67]. More work is needed to discern which of these changes, if any, con-
424 tribute to the phenotypes observed in *glp-1(Δ71)*.

425 We were initially surprised that loss of the GLD-1 or POS-1 binding motifs did not cause
426 stronger phenotypes. In fact, we expected to have difficulty recovering these mutants because
427 we anticipated strong upregulation of GLP-1, which is known to cause a gain-of-function sterility
428 phenotype where the germline forms a tumor of ectopic progenitor cells. This turned out not to be

429 the case. Mutation of all three binding sites and the adjacent regions caused an increase in the
430 amount of mitosis and a moderate expansion of the mitotic zone, but apparently the extent of
431 dysregulation observed was not enough to cause germline progenitor cell tumor formation. Per-
432 haps a larger deletion of the 3' UTR could cause a stronger phenotype. We attempted to make a
433 full 3'UTR deletion of the *glp-1* gene, but we were unable to recover this mutant, although tech-
434 nical hurdles associated with non-allelic homologous recombination with a downstream pseudo-
435 gene appears to be the root cause of this difficulty (not shown). Having said that, we note that
436 similar 3'UTR deletion alleles of key cell-fate specifying maternal genes *mex-3* and *pos-1* also do
437 not produce strong reproductive phenotypes [49, 50]. Together with the *glp-1* results reported
438 here, our work supports an emerging model where silent maternal transcripts inherited by em-
439 bryos act to buffer protein production but are not essential for fertility.

440

441 **METHODS**

442

443 *C. elegans strains and CRISPR mutagenesis*

444 All strains used in this work were cultured on NGM agar plates seeded with *E. coli* OP50
445 strain [68] under standard conditions unless otherwise noted. The strains used in this study are
446 listed in **Table 1.** CRISPR/Cas9 mutagenesis was carried out following the protocol of Ghanta et
447 al. [69]. A single crRNA and an ssODN or DNA oligonucleotide repair template unique to each
448 mutation was employed for the *glp-1::2xOLLAS* background mutations (*spr16, spr21, spr22, and*
449 *spr33*). The sequences of the crRNA, the DNA repair template, and the ssODNs are listed in
450 **Supplemental Table 1**. The offspring of injected animals were isolated, allowed to propagate,
451 then lysed and used as a template in PCR using primers F21: 5'-CGGTCAATGCGATGTGGTAT-
452 3' and R21-2: 5'-GAGCCTCGAGAATGGTGAGT-3'. For *spr16*, the presence of the deletion prod-
453 uct was visualized directly on a 2% agarose gel. For point mutations, the amplification product

454 was treated with the HindIII-HF restriction enzyme, where lack of cleavage indicated a successful
455 mutation (NEB, catalog number: R3104S, New Ipswich, MA). Cleavage products were resolved
456 on a 2% agarose gel. Sanger sequencing was used to validate the mutation after candidate ho-
457 mozygous lines were isolated. Validated mutants were outcrossed three times with the back-
458 ground strain to eliminate off target and spurious background mutations for each strain
459 respectively.

460

461 *RNAi by feeding*

462 Double-stranded DNA sequences used to target *gld-2* or *gld-4* in RNAi experiments were
463 amplified from synthetic DNA (GenScript, Piscataway, NJ). Amplicons were designed using the
464 sequences from Ahringer RNAi library [64, 70]. The *gld-2* amplicon is 1194 nucleotides (primers:
465 *gld-2*F: 5'-AGTACGGCCGTTGGTATCAG-3', *gld-2*R: 5'-ATGTTGCTGCTGATTGTTGC-3', **Sup-**
466 **plemental Table 1**), while the *gld-4* amplicon is 969 nucleotides (primers: *gld-4*F: 5'-TTTCG-
467 GAGCGAGAAGACACT-3', *gld-4*R: 5'-GTGGCTGAGTTGTTGTCGAA-3') [70, 71]. PCR products
468 were cloned into vector L4440, and RNAi experiments were carried out as described previously
469 [32, 72]. Briefly, adult worms were bleached to recover embryos, which were then placed on plates
470 with 100 µg/mL ampicillin and 1mM IPTG to induce RNAi upon hatching. Animals were cultivated
471 at 25°C until reaching the young adult stage. After dissection, embryos were placed on 2% aga-
472 rose pad and imaged under DIC optics and fluorescence optics (see below). The previously re-
473 ported phenotypes were used to confirm RNAi efficacy [44]. *pos-1* RNAi was used as a positive
474 control condition and resulted in embryonic lethality [32].

475

476 *RNAi by soaking*

477 Total RNA was isolated from one or two 60 mm plates of N2 worms using Trizol followed
478 by phenol-chloroform-isoamyl alcohol extraction. RT-PCR was performed using Superscript III
479 One-Step RT-PCR kit (ThermoFisher, catalog number: 12574026, Waltham, MA) using the pri-
480 mers listed in **Supplemental Table 1**. Primers for each of the genes of interest targeted exon-
481 exon junctions to reduce amplification of residual contaminating genomic DNA. Each primer in-
482 cludes a T7 promoter on the 5' end. The amplicons vary in length from 550 to 950 base pairs.
483 Double stranded RNA was made from the RT-PCR products using the MEGAScript T7 Transcrip-
484 tion Kit (ThermoFisher, catalog number: AM1333, Waltham, MA). Soaking solution was made
485 following the procedure of Ahringer with a final concentration of 1 μg/μl of double-stranded RNA
486 [70]. Synchronized L1 animals were incubated in this solution at 25°C for 24 hours. After transfer-
487 ring to NGM agar plates seeded with *E. coli* OP50, they were cultured at 25°C until the young
488 adult stage. Embryos were harvested by dissection for imaging under DIC and fluorescence optics
489 (see below). The previously described phenotypes for each RNAi condition were used to confirm
490 knockdown [73].

491

492 *Brood size and hatch rate assays*

493 Following synchronization, worms from each tested genotype were cultivated at room tem-
494 perature before being isolated onto NGM plates with *E. coli* OP50. Every day, each animal was
495 moved to a different plate, and the number of eggs laid and hatched progeny were counted. Three
496 biological replicates including 30-35 worms were performed for each strain and culture condition.
497 A one-way ANOVA was used to assess differences between the brood size and hatch rate (viable
498 progeny / total progeny) with Bonferroni correction for multiple hypothesis testing.

499

500 *Reporter transgene fluorescence microscopy and quantification*

501 A Zeiss Axioskop 2 plus microscope (Jena, Germany) with a 40X oil-immersion objective
502 and a Spot camera (Sterling Heights, MI) was used to collect embryo images under DIC and flu-
503 orescence optics. For embryo imaging, the mean pixel fluorescence intensity in the nucleus was
504 determined for each nucleus in all imaged four-cell embryos using FIJI v2.9.0 (https://im-
505 agej.net/software/fiji/). The reported value is the sum of the four nuclei in each four-cell embryo.
506 The mean and standard deviation of this sum was calculated for multiple embryos under each
507 treatment condition (**Fig. 2**). The data were plotted using Igor Pro9 (Wavemetrics, Portland,
508 OR); and the Tukey method was used to identify outliers. A one-way ANOVA was performed to
509 assess statistical significance, the p-value was adjusted using the Bonferroni correction for mul-
510 tiple hypothesis testing. For oocyte imaging, the background-corrected mean pixel fluorescence
511 intensity in the nucleus of the four most proximal oocytes was determined. The mean pixel in-
512 tensity of each was determined, and the reported value is the average of all four nuclei. The av-
513 erage and standard deviation from multiple worms was determined. The Tukey method was
514 used to identify outliers, and the data were compared using a one-way ANOVA to evaluate the
515 significance using the Bonferroni correction for multiple hypothesis testing.

516

517 *Immunofluorescence imaging and quantitation*

518 After slides were prepared with poly-L-lysine treatment, gonads were dissected in Happy
519 Buffer (25 mM HEPES pH7.0, 50 mM NaCl, 5 mM KCl, 2 mM $MgCl_2$ and 2mM EDTA) containing
520 0.2 mM Levamisole. The worms were fixed with the fixation buffer (2X buffer: 25 mM HEPES
521 pH7.4, 49 mM NaCl, 5 mM KCl, 2 mM $MgCl_2$, 1mM EGTA and 5% paraformaldehyde and incu-
522 bated for 30 minutes. The slides were washed with 0.2M Tris pH 7.5 twice before being incu-
523 bated in Permeabilization Buffer [PBST (0.1%), Triton (0.1%)] for 15 minutes and then
524 submerged into PBST (0.1%). After incubating with primary antibody (rat anti-OLLAS (Novus
525 #NBP1-06713) 1:500; monoclonal mouse Phospho-Histone H3 (Ser10) (6G3) (Cell Signaling

526 9706S) 1:200) overnight at 4°C, PBST (0.1%) was used twice for 5 minutes to wash the slides,
527 which was followed by the secondary antibody (AlexaFluor 488 donkey anti-rat (Invitrogen
528 #A21208, headquarters: Carlsbad, CA) 1:500 dilution; Rhodamine Red™-X (RRX) AffiniPure
529 Goat Anti-Mouse IgG (H+L) (Jackson ImmunoResearch 115-295-003, West Grove, PA) 1:200
530 dilution) treatment for 2 hours at room temperature. PBST (0.1%) was used twice to rinse the
531 slides, then Vectashield Antifade Medium (Vector Labs, Newark, CA) containing DAPI was used
532 to mount the gonads on the slide, covered with a coverslip, sealed with clear nail polish and al-
533 lowed to dry for half an hour. Fluorescent microscopy was used to image the slides.

534 Images were collected on a Zeiss AxioObserver 7 inverted imaging system (model num-
535 ber:431007-9904-000, serial number:3858002009, Oberkochen, Germany) with 20X air and/or
536 40X oil objectives under DIC and fluorescence optics. Z-stacks of 30 images spanning the width
537 of the gonads were collected using the green channel for OLLAS, the red channel for PH-3, and
538 the blue channel for DAPI, and DIC for light microscopy. The images were quantified using Fiji
539 version 2.14.0. The lengths of the mitotic zone and the length of the OLLAS-positive region
540 were measured using the segmented line tool. The ollas immunofluorescence intensity was de-
541 termined using the circle tool with radius of 30 pixels and normalized to an equivalent circle out-
542 side of the gonad to correct for background. The statistical significance was determined using a
543 one-way ANOVA with Bonferroni correction for multiple hypothesis testing.

544

545 *Analysis of polyA-test sequencing data (PAT-Seq)*

546 Raw sequencing reads from published polyA-test sequencing data corresponding to NIH
547 Bioproject PRJNA248698 were downloaded from the NIH Sequence Read Archive [41]. Reads
548 that correspond to *glp-1* isoforms were recovered from the raw data using the fuzzy pattern search
549 algorithm ugrep v7.4.1 (https://github.com/Genivia/ugrep) built into a custom script

550 (**Supplementary Data Set 3**). The pattern used for the search consists of 1) a 20 nucleotide long
551 3'UTR isoform specific search term near the polyA processing site (search1 = 5'-
552 CTCGGTTCATTTTAAATATG-3'; search2 = 5'-CATTTTTCTTATTCTAGACT-3'; search3 =
553 TCCTTTTCTTTATAACTTGT-3'; search4 = 5'-CATTTAATGAATTGTAATTC-3'; search5 = 5'-
554 AGATTAAGAGTATAAGCTTT-3'; search6 = 5'-TTCGAATTATTGAAGCTCAA-3'), 2) a variable
555 length gap ranging from 0 to 10 nucleotides, 3) a stretch of continuous adenosines at least five
556 nucleotides long, and 4) eight nucleotides of the tag sequence used to clone the polyA tails during
557 library construction (GATCGGAA) [74]. The advantage of ugrep compared to similar grep-based
558 search algorithms is that it can search for near matches. We ran our script with 0-3 possible
559 mismatches compared to our search expression and found that 2 or 3 mismatches permitted the
560 recovery of reads that do not correspond to *glp-1*, while 0 or 1 errors produced only matches to
561 *glp-1* and comparable results (**Fig. 2, Supplemental Data Set 3**). The length of the polyA tail was
562 counted using a second iteration of ugrep to recover the polyA tail with the 3' tag, and awk
563 v.20200816 was used to count the length of the polyA tail. The full script with list of commands
564 and the output is available in **Supplemental Data Set 3**. The number of isoform-specific reads
565 was divided by the total number of *glp-1* reads to determine the fraction of polyA tails associated
566 with a particular UTR isoform. The mean, median, and standard deviation of each distribution was
567 calculated. A non-parametric Komolgorov-Smirnov (KS) test was used to evaluate apparent dif-
568 ferences between distributions, and p-values were adjusted for multiple hypothesis testing using
569 the Bonferroni correction.

570

571 *Reporter transgene PolyA tail length measurements*

572 Young adult animals were washed with M9 several times, centrifuged, and resuspended
573 in Trizol (Invitrogen, catalog number: 15596018, Carlsbad, CA), frozen and stored at -80°C. To
574 isolate embryos, young adult animals were bleached with hypochlorite solution, washed with M9,

575 centrifuged, resuspended in Trizol, frozen and stored at -80°C. RNA was isolated by using phenol-
576 chloroform extraction method. PolyA tail length measurements were conducted as published with
577 a few changes [45]. Superscript III One-Step RT-PCR kit (ThermoFisher, catalog number:
578 12574026, Waltham, MA) was utilized after the guanosine and inosine extension step [45]. The
579 PCR fragments were run on agarose gel. Primers used in this assay: C10T2 (sequence: 5'-
580 CCCCCCCCCCTT-3') to make cDNA, M13RC0T2 (sequence: 5'-CAGGAAACAGC-
581 TATGACCCCCCCCCCCTT-3') [45] to amplify the tail, forward primer (sequence: 5'-
582 GCGATGGCCCTGTCCTTTTA-3') to amplify both transcripts, reverse primer for the gene (se-
583 quence: 5'-GGGACCAGTGTCTGGGTGATGT-3') to amplify only gene specific transcripts. TOPO
584 Cloning was performed using StrataClone PCR Cloning Kit manual (Agilent, catalog number:
585 240205), which was followed by Sanger sequencing by Elim Biopharm (Hayward, CA) or Eton
586 Bioscience (San Diego, CA). The polyA tail length for each isolate was counted directly from the
587 sequencing results and plotted as a function of genotype. The mean, median, and standard devi-
588 ation of each genotype and age group was calculated, and differences in the distributions were
589 assessed by a non-parametric KS test with Bonferroni correction for multiple hypothesis testing.

590

591 *Terminal embryo phenotyping*

592 Embryos from *glp-1(WT)*, *glp-1(Δ71)*, and *glp-1(ts)* strains were recovered by washing
593 them off NGM agar plates with M9 followed by bleaching in hypochlorite solution (20% bleach,
594 0.25M NaOH final concentration). After washing with extensively with M9, one drop of embryos
595 in M9 solution was placed on a 2% agarose pad on a microscope slide, covered with a cover slip,
596 and imaged under DIC optics using a Zeiss Axiobserver 7 imaging system described above with
597 a 63X oil immersion objective. The embryos were assessed as a function of developmental stage
598 and defined as “normal” or “abnormal” based upon their appearance. The cross-tabulation Chi-

599 square method was used to assess statistical significance, and p-values were adjusted for multi-
600 ple hypothesis testing using the Bonferroni correction for multiple hypothesis testing.

601

602 *RNA-seq library preparation*

603 *glp-1::2xOLLAS*, *glp-1(spr16), glp-1(spr21)*, *glp-1(spr22)* and *glp-1(spr33)* strains were
604 synchronized by bleaching followed by hatching in M9 and arrest at the L1 stage. L1 animals were
605 cultivated in an incubator at 20°C on NGM agar seeded with *E. coli* OP50 until they reached the
606 young adult stage. Embryos were allowed to hatch overnight, leading to arrest at L1 stage. L1
607 animals were plated on NGM agar with *E. coli* OP50 and cultured in an incubator at 20°C until
608 they reached the young adult stage. The worms were collected for RNA isolation by washing them
609 off with M9 several times, and any extra M9 was removed. After addition of 1 mL Trizol, they were
610 frozen at -80 °C. Phenol-chloroform extraction was used to isolate the RNA and depletion of ribo-
611 somal RNA was carried out following the procedure of Duan et al. [75]. Sample concentrations
612 were determined using a Qubit fluorometer (ThermoFisher, Waltham, MA) and the RNA quality
613 was assessed using a Bioanalyzer (Agilent, Santa Clara, CA). The NEBNext Ultra II RNA Library
614 Prep kit (NEB catalog number: E7775S, New Ipswich, MA) was used to prepare the RNA-seq
615 libraries. The libraries were indexed using NEBNext Multiplex Oligos for Illumina (Dual Index Pri-
616 mer Sets 1, 2, 3, and 4) (catalog numbers: E7600S, E7780S, E7710S, and E7730S). An Illumina
617 NextSeq 500 was used to sequence the final pooled libraries. Three biological replicates were
618 gathered for *glp-1(spr21)*, *glp-1(spr22)* and *glp-1(spr33)*, and two biological replicates for *glp-*
619 *1::2xOLLAS*, *glp-1(spr16)*.

620 The OneStopRNAseq v1.0.0 pipeline was utilized for RNA-seq analysis, and the reads
621 were aligned using the reference genome WBcel235 [53]. The differential gene expression was
622 examined using the DESeq2_1.28.1 tool [54]. Cutoffs for differential expression were an absolute

log2 fold change of greater than 0.585 and an FDR was less than 0.05. WormCat was used to evaluate gene function categories in differentially expressed genes [76].

Data availability

All numerical data and statistical analyses presented in this report are available in **Supplementary Data Set 1**. The output of the OneStopRNASeq pipeline, the Wormcat analysis, and the tissue enrichment analysis described in **Figure 7** are included as **Supplementary Data Set 2.** The custom scripts used to measure polyA tail length in **Figure 2**, and all output from the scripts, are included as **Supplementary Data Set 3**. Raw RNA sequencing data were uploaded to the NIH Sequence Read Archive and will be made available under Bioproject PRJNA1440940. All imaging data is available through Zenodo (DOI: 10.5281/zenodo.19183906).

ACKNOWLEDGEMENTS

The authors thank Nick Rhind, Oliver Rando, Craig Mello, and Victor Ambros for sharing reagents and/or their advice on data analysis and interpretation. We thank Sharon Noronha and Haik Varderesian for helpful comments on the manuscript. This work was supported by NIH Grant R01GM145062 to S.P.R.

AUTHOR CONTRIBUTIONS

PC collected all the data presented in the manuscript and made strains WRM73, WRM83, WRM84, and WRM109. PC analyzed the data with the following exceptions—SR assisted with some quantitation and statistical analyses described in Figures 2–4, and 6. All experiments were conceived by PC and SR, and both authors prepared the manuscript.

646 ## REFERENCES

647 1. Kojima ML, Hoppe C, Giraldez AJ. The maternal-to-zygotic transition: reprogramming of
648 the cytoplasm and nucleus. Nat Rev Genet. 2025;26(4):245-67. Epub 2024/11/26. doi:
649 10.1038/s41576-024-00792-0. PubMed PMID: 39587307; PubMed Central PMCID:
650 PMC11928286.
651 2. Farley BM, Ryder SP. Regulation of maternal mRNAs in early development. Crit Rev
652 Biochem Mol Biol. 2008;43(2):135-62. Epub 2008/03/28. doi:
653 10.1080/10409230801921338. PubMed PMID: 18365862.
654 3. Bowerman B, Eaton BA, Priess JR. skn-1, a maternally expressed gene required to
655 specify the fate of ventral blastomeres in the early C. elegans embryo. Cell.
656 1992;68(6):1061-75. Epub 1992/03/20. PubMed PMID: 1547503.
657 4. Evans TC, Crittenden SL, Kodoyianni V, Kimble J. Translational control of maternal glp-1
658 mRNA establishes an asymmetry in the C. elegans embryo. Cell. 1994;77(2):183-94.
659 Epub 1994/04/22. PubMed PMID: 8168128.
660 5. Mango SE, Thorpe CJ, Martin PR, Chamberlain SH, Bowerman B. Two maternal genes,
661 apx-1 and pie-1, are required to distinguish the fates of equivalent blastomeres in the
662 early Caenorhabditis elegans embryo. Development. 1994;120(8):2305-15. Epub
663 1994/08/01. PubMed PMID: 7925031.
664 6. Hunter CP, Kenyon C. Spatial and temporal controls target pal-1 blastomere-
665 specification activity to a single blastomere lineage in C. elegans embryos. Cell.
666 1996;87(2):217-26.
667 7. Tintori SC, Osborne Nishimura E, Golden P, Lieb JD, Goldstein B. A Transcriptional
668 Lineage of the Early C. elegans Embryo. Dev Cell. 2016;38(4):430-44. Epub 2016/08/25.
669 doi: 10.1016/j.devcel.2016.07.025. PubMed PMID: 27554860; PubMed Central PMCID:
670 PMC4999266.

671 8. Robertson S, Lin R. The Maternal-to-Zygotic Transition in C. elegans. Curr Top Dev Biol.
672 2015;113:1-42. Epub 2015/09/12. doi: 10.1016/bs.ctdb.2015.06.001. PubMed PMID:
673 26358869.
674 9. Batchelder C, Dunn MA, Choy B, Suh Y, Cassie C, Shim EY, et al. Transcriptional
675 repression by the Caenorhabditis elegans germ-line protein PIE-1. Genes Dev.
676 1999;13(2):202-12. Epub 1999/01/30. doi: 10.1101/gad.13.2.202. PubMed PMID:
677 9925644; PubMed Central PMCID: PMC316391.
678 10. Francis R, Barton MK, Kimble J, Schedl T. gld-1, a tumor suppressor gene required for
679 oocyte development in Caenorhabditis elegans. Genetics. 1995;139(2):579-606. Epub
680 1995/02/01. PubMed PMID: 7713419; PubMed Central PMCID: PMC1206368.
681 11. Draper BW, Mello CC, Bowerman B, Hardin J, Priess JR. MEX-3 is a KH domain protein
682 that regulates blastomere identity in early C-elegans embryos. Cell. 1996;87(2):205-16.
683 PubMed PMID: ISI:A1996VN40300009.
684 12. Tabara H, Hill RJ, Mello CC, Priess JR, Kohara Y. pos-1 encodes a cytoplasmic zinc-
685 finger protein essential for germline specification in C. elegans. Development.
686 1999;126(1):1-11. Epub 1998/12/03. PubMed PMID: 9834181.
687 13. Olivas W, Parker R. The Puf3 protein is a transcript-specific regulator of mRNA
688 degradation in yeast. Embo J. 2000;19(23):6602-11.
689 14. Gomes JE, Encalada SE, Swan KA, Shelton CA, Carter JC, Bowerman B. The maternal
690 gene spn-4 encodes a predicted RRM protein required for mitotic spindle orientation and
691 cell fate patterning in early C. elegans embryos. Development. 2001;128(21):4301-14.
692 Epub 2001/10/31. PubMed PMID: 11684665.
693 15. Albarqi MMY, Ryder SP. The role of RNA-binding proteins in orchestrating germline
694 development in Caenorhabditis elegans. Front Cell Dev Biol. 2022;10:1094295. Epub
695 2023/01/24. doi: 10.3389/fcell.2022.1094295. PubMed PMID: 36684428; PubMed
696 Central PMCID: PMC9846511.

697 16. Merritt C, Rasoloson D, Ko D, Seydoux G. 3' UTRs are the primary regulators of gene
698 expression in the C. elegans germline. Curr Biol. 2008;18(19):1476-82. Epub
699 2008/09/27. doi: 10.1016/j.cub.2008.08.013. PubMed PMID: 18818082; PubMed Central
700 PMCID: PMC2585380.
701 17. Allen MA, Hillier LW, Waterston RH, Blumenthal T. A global analysis of C. elegans trans-
702 splicing. Genome Res. 2011;21(2):255-64. Epub 2010/12/24. doi:
703 10.1101/gr.113811.110. PubMed PMID: 21177958; PubMed Central PMCID:
704 PMC3032929.
705 18. Austin J, Kimble J. glp-1 is required in the germ line for regulation of the decision
706 between mitosis and meiosis in C. elegans. Cell. 1987;51(4):589-99. Epub 1987/11/20.
707 PubMed PMID: 3677168.
708 19. Henderson ST, Gao D, Lambie EJ, Kimble J. lag-2 may encode a signaling ligand for the
709 GLP-1 and LIN-12 receptors of C. elegans. Development. 1994;120(10):2913-24. Epub
710 1994/10/01. doi: 10.1242/dev.120.10.2913. PubMed PMID: 7607081.
711 20. Doyle TG, Wen C, Greenwald I. SEL-8, a nuclear protein required for LIN-12 and GLP-1
712 signaling in Caenorhabditis elegans. Proc Natl Acad Sci U S A. 2000;97(14):7877-81.
713 Epub 2000/07/08. doi: 10.1073/pnas.97.14.7877. PubMed PMID: 10884418; PubMed
714 Central PMCID: PMC16638.
715 21. Mickey KM, Mello CC, Montgomery MK, Fire A, Priess JR. An inductive interaction in 4-
716 cell stage C. elegans embryos involves APX-1 expression in the signalling cell.
717 Development. 1996;122(6):1791-8.
718 22. Priess JR, Schnabel H, Schnabel R. The glp-1 locus and cellular interactions in early C.
719 elegans embryos. Cell. 1987;51(4):601-11. Epub 1987/11/20. PubMed PMID: 3677169.
720 23. Mello CC, Draper BW, Priess JR. The maternal genes apx-1 and glp-1 and
721 establishment of dorsal-ventral polarity in the early C. elegans embryo. Cell.
722 1994;77(1):95-106. Epub 1994/04/08. PubMed PMID: 8156602.

723 24. Crittenden SL, Rudel D, Binder J, Evans TC, Kimble J. Genes required for GLP-1
724 asymmetry in the early Caenorhabditis elegans embryo. Dev Biol. 1997;181(1):36-46.
725 25. Pagano JM, Farley BM, Essien KI, Ryder SP. RNA recognition by the embryonic cell fate
726 determinant and germline totipotency factor MEX-3. Proc Natl Acad Sci U S A.
727 2009;106(48):20252-7. doi: 10.1073/pnas.0907916106. PubMed PMID: 19915141;
728 PubMed Central PMCID: PMC2787150.
729 26. Kaymak E, Ryder SP. RNA recognition by the Caenorhabditis elegans oocyte maturation
730 determinant OMA-1. J Biol Chem. 2013;288(42):30463-72. doi:
731 10.1074/jbc.M113.496547. PubMed PMID: 24014033; PubMed Central PMCID:
732 PMC3798510.
733 27. Tamburino AM, Kaymak E, Shrestha S, Holdorf AD, Ryder SP, Walhout AJM. PRIMA: a
734 gene-centered, RNA-to-protein method for mapping RNA-protein interactions.
735 Translation (Austin). 2017;5(1):e1295130. doi: 10.1080/21690731.2017.1295130.
736 PubMed PMID: 28702278; PubMed Central PMCID: PMC5501385.
737 28. Lublin AL, Evans TC. The RNA-binding proteins PUF-5, PUF-6, and PUF-7 reveal
738 multiple systems for maternal mRNA regulation during C. elegans oogenesis. Dev Biol.
739 2007;303(2):635-49. Epub 2007/01/20. doi: 10.1016/j.ydbio.2006.12.004. PubMed
740 PMID: 17234175.
741 29. Marin VA, Evans TC. Translational repression of a C. elegans Notch mRNA by the
742 STAR/KH domain protein GLD-1. Development. 2003;130(12):2623-32. Epub
743 2003/05/09. PubMed PMID: 12736207.
744 30. Ogura K, Kishimoto N, Mitani S, Gengyo-Ando K, Kohara Y. Translational control of
745 maternal glp-1 mRNA by POS-1 and its interacting protein SPN-4 in Caenorhabditis
746 elegans. Development. 2003;130(11):2495-503. Epub 2003/04/19. doi:
747 10.1242/dev.00469. PubMed PMID: 12702662.

748 31. Pagano JM, Farley BM, McCoig LM, Ryder SP. Molecular basis of RNA recognition by
749 the embryonic polarity determinant MEX-5. J Biol Chem. 2007;282(12):8883-94. doi:
750 10.1074/jbc.M700079200. PubMed PMID: 17264081.
751 32. Farley BM, Ryder SP. POS-1 and GLD-1 repress glp-1 translation through a conserved
752 binding-site cluster. Mol Biol Cell. 2012;23(23):4473-83. Epub 2012/10/05. doi:
753 10.1091/mbc.E12-03-0216. PubMed PMID: 23034181; PubMed Central PMCID:
754 PMC3510010.
755 33. Ryder SP, Frater LA, Abramovitz DL, Goodwin EB, Williamson JR. RNA target specificity
756 of the STAR/GSG domain post-transcriptional regulatory protein GLD-1. Nat Struct Mol
757 Biol. 2004;11(1):20-8. doi: 10.1038/nsmb706. PubMed PMID: 14718919.
758 34. Jungkamp AC, Stoeckius M, Mecenas D, Grun D, Mastrobuoni G, Kempa S, et al. In
759 vivo and transcriptome-wide identification of RNA binding protein target sites. Mol Cell.
760 2011;44(5):828-40. Epub 2011/12/14. doi: 10.1016/j.molcel.2011.11.009. PubMed PMID:
761 22152485; PubMed Central PMCID: PMC3253457.
762 35. Wright JE, Gaidatzis D, Senften M, Farley BM, Westhof E, Ryder SP, et al. A quantitative
763 RNA code for mRNA target selection by the germline fate determinant GLD-1. EMBO J.
764 2011;30(3):533-45. doi: 10.1038/emboj.2010.334. PubMed PMID: 21169991; PubMed
765 Central PMCID: PMC3034010.
766 36. Scheckel C, Gaidatzis D, Wright JE, Ciosk R. Genome-Wide Analysis of GLD-1-
767 Mediated mRNA Regulation Suggests a Role in mRNA Storage. PLoS Genet.
768 2012;8(5):e1002742. Epub 2012/06/14. doi: 10.1371/journal.pgen.1002742. PubMed
769 PMID: 22693456; PubMed Central PMCID: PMC3364957.
770 37. Farley BM, Pagano JM, Ryder SP. RNA target specificity of the embryonic cell fate
771 determinant POS-1. RNA. 2008;14(12):2685-97. doi: 10.1261/rna.1256708. PubMed
772 PMID: 18952820; PubMed Central PMCID: PMC2590972.

773 38. Elkon R, Ugalde AP, Agami R. Alternative cleavage and polyadenylation: extent,
774 regulation and function. Nat Rev Genet. 2013;14(7):496-506. doi: 10.1038/nrg3482.
775 PubMed PMID: 23774734.
776 39. Mangone M, Manoharan AP, Thierry-Mieg D, Thierry-Mieg J, Han T, Mackowiak SD, et
777 al. The landscape of C. elegans 3'UTRs. Science. 2010;329(5990):432-5. Epub
778 2010/06/05. doi: 10.1126/science.1191244. PubMed PMID: 20522740; PubMed Central
779 PMCID: PMC3142571.
780 40. Jan CH, Friedman RC, Ruby JG, Bartel DP. Formation, regulation and evolution of
781 Caenorhabditis elegans 3'UTRs. Nature. 2011;469(7328):97-101. Epub 2010/11/19. doi:
782 10.1038/nature09616. PubMed PMID: 21085120; PubMed Central PMCID:
783 PMC3057491.
784 41. Elewa A, Shirayama M, Kaymak E, Harrison PF, Powell DR, Du Z, et al. POS-1
785 Promotes Endo-mesoderm Development by Inhibiting the Cytoplasmic Polyadenylation
786 of neg-1 mRNA. Dev Cell. 2015;34(1):108-18. doi: 10.1016/j.devcel.2015.05.024.
787 PubMed PMID: 26096734; PubMed Central PMCID: PMC4507413.
788 42. Lima SA, Chipman LB, Nicholson AL, Chen YH, Yee BA, Yeo GW, et al. Short poly(A)
789 tails are a conserved feature of highly expressed genes. Nat Struct Mol Biol.
790 2017;24(12):1057-63. Epub 2017/11/07. doi: 10.1038/nsmb.3499. PubMed PMID:
791 29106412; PubMed Central PMCID: PMC5877826.
792 43. Eckmann CR, Kraemer B, Wickens M, Kimble J. GLD-3, a Bicaudal-C homolog that
793 inhibits FBF to control germline sex determination in C-elegans. Developmental Cell.
794 2002;3(5):697-710. PubMed PMID: ISI:000179230900012.
795 44. Wang L, Eckmann CR, Kadyk LC, Wickens M, Kimble J. A regulatory cytoplasmic
796 poly(A) polymerase in Caenorhabditis elegans. Nature. 2002;419(6904):312-6.

797 45. Patil DP, Bakthavachalu B, Schoenberg DR. Poly(A) polymerase-based poly(A) length
798 assay. Methods Mol Biol. 2014;1125:13-23. Epub 2014/03/05. doi: 10.1007/978-1-
799 62703-971-0_2. PubMed PMID: 24590776; PubMed Central PMCID: PMC3951053.
800 46. Schmid M, Kuchler B, Eckmann CR. Two conserved regulatory cytoplasmic poly(A)
801 polymerases, GLD-4 and GLD-2, regulate meiotic progression in C. elegans. Genes
802 Dev. 2009;23(7):824-36. doi: 10.1101/gad.494009. PubMed PMID: 19339688; PubMed
803 Central PMCID: PMC2666339.
804 47. Nousch M, Yeroslaviz A, Habermann B, Eckmann CR. The cytoplasmic poly(A)
805 polymerases GLD-2 and GLD-4 promote general gene expression via distinct
806 mechanisms. Nucleic Acids Res. 2015;42(18):11622-33. doi: 10.1093/nar/gku838.
807 PubMed PMID: 25217583.
808 48. Sorensen EB, Seidel HS, Crittenden SL, Ballard JH, Kimble J. A toolkit of tagged glp-1
809 alleles reveals strong glp-1 expression in the germline, embryo, and spermatheca.
810 MicroPubl Biol. 2020;2020. Epub 2020/07/07. doi: 10.17912/micropub.biology.000271.
811 PubMed PMID: 32626848; PubMed Central PMCID: PMC7326335.
812 49. Brown HE, Varderesian HV, Keane SA, Ryder SP. The mex-3 3' untranslated region is
813 essential for reproduction during temperature stress. bioRxiv. 2025. Epub 2025/02/20.
814 doi: 10.1101/2024.04.01.587367v2. PubMed PMID: 38798418; PubMed Central PMCID:
815 PMC11123400.
816 50. Varderesian HV, Utaegbulam JN, Brown HE, Ramirez B, Velcani M, Ryder SP. The pos-1
817 3' untranslated region governs germline specification and proliferation to ensure
818 reproductive robustness. bioRxiv. 2025. Epub 2025/12/17. doi:
819 10.1101/2025.11.26.690476. PubMed PMID: 41404608; PubMed Central PMCID:
820 PMC12703999.
821 51. Berry LW, Westlund B, Schedl T. Germ-line tumor formation caused by activation of glp-
822 1, a Caenorhabditis elegans member of the Notch family of receptors. Development.

1997;124(4):925-36. Epub 1997/02/01. doi: 10.1242/dev.124.4.925. PubMed PMID: 9043073.

52. Lui DY, Colaiácovo MP. Meiotic development in Caenorhabditis elegans. Adv Exp Med Biol. 2013;757:133-70. Epub 2012/08/09. doi: 10.1007/978-1-4614-4015-4_6. PubMed PMID: 22872477; PubMed Central PMCID: PMC3764601.

53. Li R, Hu K, Liu H, Green MR, Zhu LJ. OneStopRNAseq: A Web Application for Comprehensive and Efficient Analyses of RNA-Seq Data. Genes (Basel). 2020;11(10). Epub 2020/10/08. doi: 10.3390/genes11101165. PubMed PMID: 33023248; PubMed Central PMCID: PMC7650687.

54. Love MI, Huber W, Anders S. Moderated estimation of fold change and dispersion for RNA-seq data with DESeq2. Genome Biol. 2014;15(12):550. Epub 2014/12/18. doi: 10.1186/s13059-014-0550-8. PubMed PMID: 25516281; PubMed Central PMCID: PMC4302049.

55. Higgins DP, Weisman CM, Lui DS, D'Agostino FA, Walker AK. Defining characteristics and conservation of poorly annotated genes in Caenorhabditis elegans using WormCat 2.0. Genetics. 2022;221(4). Epub 2022/05/20. doi: 10.1093/genetics/iyac085. PubMed PMID: 35587742; PubMed Central PMCID: PMC9339291.

56. Angeles-Albores D, RY NL, Chan J, Sternberg PW. Tissue enrichment analysis for C. elegans genomics. BMC Bioinformatics. 2016;17(1):366. Epub 2016/09/14. doi: 10.1186/s12859-016-1229-9. PubMed PMID: 27618863; PubMed Central PMCID: PMC5020436.

57. Huggins HP, Subash JS, Stoffel H, Henderson MA, Hoffman JL, Buckner DS, et al. Distinct roles of two eIF4E isoforms in the germline of Caenorhabditis elegans. J Cell Sci. 2020;133(6). Epub 2020/02/23. doi: 10.1242/jcs.237990. PubMed PMID: 32079657; PubMed Central PMCID: PMC7132772.

848 58. Calvo AC, Pey AL, Ying M, Loer CM, Martinez A. Anabolic function of phenylalanine
849 hydroxylase in Caenorhabditis elegans. FASEB journal : official publication of the
850 Federation of American Societies for Experimental Biology. 2008;22(8):3046-58. Epub
851 2008/05/08. doi: 10.1096/fj.08-108522. PubMed PMID: 18460651.
852 59. Harris TR, Aronov PA, Jones PD, Tanaka H, Arand M, Hammock BD. Identification of two
853 epoxide hydrolases in Caenorhabditis elegans that metabolize mammalian lipid signaling
854 molecules. Archives of biochemistry and biophysics. 2008;472(2):139-49. Epub
855 2008/02/13. doi: 10.1016/j.abb.2008.01.016. PubMed PMID: 18267101; PubMed Central
856 PMCID: PMC2435305.
857 60. Shaye DD, Greenwald I. OrthoList: a compendium of C. elegans genes with human
858 orthologs. PLoS One. 2011;6(5):e20085. Epub 2011/06/08. doi:
859 10.1371/journal.pone.0020085. PubMed PMID: 21647448; PubMed Central PMCID:
860 PMC3102077.
861 61. Dong B, Valencia CA, Liu R. Ca(2+)/calmodulin directly interacts with the pleckstrin
862 homology domain of AKT1. J Biol Chem. 2007;282(34):25131-40. Epub 2007/06/21. doi:
863 10.1074/jbc.M702123200. PubMed PMID: 17580302.
864 62. Okahata M, Sawada N, Nakao K, Ohta A, Kuhara A. Screening for cold tolerance genes
865 in C. elegans, whose expressions are affected by anticancer drugs camptothecin and
866 leptomycin B. Scientific reports. 2024;14(1):5401. Epub 2024/03/06. doi:
867 10.1038/s41598-024-55794-z. PubMed PMID: 38443452; PubMed Central PMCID:
868 PMC10914781.
869 63. Karplus K, Barrett C, Hughey R. Hidden Markov models for detecting remote protein
870 homologies. Bioinformatics. 1998;14(10):846-56. Epub 1999/02/03. PubMed PMID:
871 9927713.

872 64. Kamath RS, Fraser AG, Dong Y, Poulin G, Durbin R, Gotta M, et al. Systematic
873 functional analysis of the Caenorhabditis elegans genome using RNAi. Nature.
874 2003;421(6920):231-7.
875 65. Alper S, Laws R, Lackford B, Boyd WA, Dunlap P, Freedman JH, et al. Identification of
876 innate immunity genes and pathways using a comparative genomics approach. Proc
877 Natl Acad Sci U S A. 2008;105(19):7016-21. Epub 2008/05/09. doi:
878 10.1073/pnas.0802405105. PubMed PMID: 18463287; PubMed Central PMCID:
879 PMC2383967.
880 66. Sundaram P, Echalier B, Han W, Hull D, Timmons L. ATP-binding cassette transporters
881 are required for efficient RNA interference in Caenorhabditis elegans. Mol Biol Cell.
882 2006;17(8):3678-88. Epub 2006/05/26. doi: 10.1091/mbc.e06-03-0192. PubMed PMID:
883 16723499; PubMed Central PMCID: PMC1525249.
884 67. Huang LS, Tzou P, Sternberg PW. The lin-15 locus encodes two negative regulators of
885 Caenorhabditis elegans vulval development. Mol Biol Cell. 1994;5(4):395-411. Epub
886 1994/04/01. doi: 10.1091/mbc.5.4.395. PubMed PMID: 8054684; PubMed Central
887 PMCID: PMC301050.
888 68. Brenner S. The genetics of Caenorhabditis elegans. Genetics. 1974;77(1):71-94. Epub
889 1974/05/01. PubMed PMID: 4366476; PubMed Central PMCID: PMC1213120.
890 69. Ghanta KS, Mello CC. Melting dsDNA Donor Molecules Greatly Improves Precision
891 Genome Editing in Caenorhabditis elegans. Genetics. 2020;216(3):643-50. Epub
892 2020/09/24. doi: 10.1534/genetics.120.303564. PubMed PMID: 32963112; PubMed
893 Central PMCID: PMC7648581.
894 70. Fraser AG, Kamath RS, Zipperlen P, Martinez-Campos M, Sohrmann M, Ahringer J.
895 Functional genomic analysis of C. elegans chromosome I by systematic RNA
896 interference. Nature. 2000;408(6810):325-30.

897 71. Kamath RS, Ahringer J. Genome-wide RNAi screening in Caenorhabditis elegans.
898 Methods. 2003;30(4):313-21.
899 72. Conte D, Jr., Mello CC. RNA interference in Caenorhabditis elegans. Current protocols in
900 molecular biology / edited by Frederick M Ausubel [et al]. 2003;Chapter 26:Unit 26 3.
901 Epub 2008/02/12. doi: 10.1002/0471142727.mb2603s62. PubMed PMID: 18265327.
902 73. Keiper BD, Lamphear BJ, Deshpande AM, Jankowska-Anyszka M, Aamodt EJ,
903 Blumenthal T, et al. Functional characterization of five eIF4E isoforms in Caenorhabditis
904 elegans. J Biol Chem. 2000;275(14):10590-6. Epub 2000/04/01. doi:
905 10.1074/jbc.275.14.10590. PubMed PMID: 10744754.
906 74. Harrison PF, Powell DR, Clancy JL, Preiss T, Boag PR, Traven A, et al. PAT-seq: a
907 method to study the integration of 3'-UTR dynamics with gene expression in the
908 eukaryotic transcriptome. Rna. 2015;21(8):1502-10. Epub 2015/06/21. doi:
909 10.1261/rna.048355.114. PubMed PMID: 26092945; PubMed Central PMCID:
910 PMC4509939.
911 75. Duan Y, Sun Y, Ambros V. RNA-seq with RNase H-based ribosomal RNA depletion
912 specifically designed for C. elegans. MicroPubl Biol. 2020;2020. Epub 2020/10/03. doi:
913 10.17912/micropub.biology.000312. PubMed PMID: 33005886; PubMed Central PMCID:
914 PMC7520128.
915 76. Holdorf AD, Higgins DP, Hart AC, Boag PR, Pazour GJ, Walhout AJM, et al. WormCat:
916 An Online Tool for Annotation and Visualization of Caenorhabditis elegans Genome-
917 Scale Data. Genetics. 2020;214(2):279-94. Epub 2019/12/08. doi:
918 10.1534/genetics.119.302919. PubMed PMID: 31810987; PubMed Central PMCID:
919 PMC7017019.

920

921

FIGURE LEGENDS

Fig. 1. Expression pattern and 3'UTR diagram of *glp-1*. **A.** Anatomy of an adult hermaphrodite germline. The pattern of *glp-1* mRNA is shown in light orange. This image is modified from our previous figure published in [15] under the CC BY license. **B.** The pattern of GLP-1 protein is shown in the germline and early embryos in green. **C.** Diagram of the *glp-1* 3'UTR, with a map of both confirmed binding sites for POS-1 (pink) and GLD-1 (blue), as well as predicted sites matching motifs recognized by FBF (gray) or MEX-3 (purple).

Fig. 2. UTR isoform and polyA tail analysis of *glp-1* and *glp-1* 3'UTR reporter transcripts. **A.** The *glp-1* 3'UTR isoforms that can be formed by alternative polyadenylation are shown. We only observe isoform D (green) in our analysis of endogenous and reporter transcripts. The location of binding sites for POS-1 (pink) and GLD-1 (blue) is shown with dashed lines. **B.** Box plot of the polyA tail length distributions of endogenous *glp-1* polyA transcripts in embryos as a function of various RBP knock downs or mutants. The data are from genome wide PAT-test data published by Elewa et al. and available in Bioproject PRJNA248698 [41]. Each gray circle represents the polyA tail length from a *glp-1* read in the sequencing library (see methods). Asterisks represent near Tukey outliers, and “X” denotes far Tukey outliers (near outliers are 1.5X larger or smaller than the inner quartile range, far outliers are 3x). Whiskers represent the full range of the data. The number of reads analyzed is shown below. The horizontal line represents the median tail length. **C.** Diagram of the *glp-1* 3'UTR reporter transgenes used in this study (top) [32]. The mutations present in each strain are shown in red. The assay design for polyA tail length distribution measurements of the reporter transgenes is shown (bottom). Red arrows indicate gene and tail specific primer sets. The letter “I” indicates inosine. **D.** Box plot of the polyA tail distributions of the *glp-1* 3'UTR reporter transgenes from PAT assays outlined in (C). Each gray circle indicates the length of a polyA tail from an individual Sanger sequencing read. The number of colonies

947 sequenced is shown below. The median, near and far outliers, and the full range of the data are
948 shown as in (B). The color scheme for each reporter transgene variant follows the colors used in
949 panel C. Dashed lines and black asterisks indicate statistically significant differences between the
950 indicated distributions in a one-way ANOVA with Bonferroni multiple hypothesis correction (p_{adj} <
951 0.05).

952

953 **Fig. 3** Impact of post-transcriptional regulatory mechanisms on *glp-1* 3'UTR reporter transgene
954 expression. **A.** Diagram of a 4-cell embryo with the pattern of GLP-1 protein (green) and mRNA
955 (light blue) shown (left). DIC (top) and GFP (bottom) images of 4-cell embryos recovered from
956 each of the *glp-1* 3'UTR reporter transgenes [32]. **B.** Violin plots of the fluorescence intensity of
957 each 4-cell embryo from each strain under control RNAi treatment. Each gray circle represents a
958 unique embryo. The horizontal black line represents the mean. Asterisks indicate statistically sig-
959 nificant increases in a one-way ANOVA with Bonferroni correction for multiple hypothesis testing
960 (p_{adj} < 0.05). The color scheme for each variant follows figure 2C. The total number of 4-cell em-
961 bryos imaged is shown below. **C.** Same as in B, except control (ctl), *gld-2*, and *gld-4* RNAi are
962 used with the WT UTR reporter. **D.** Same as in C, except with the GBM mutant UTR reporter, and
963 double asterisks indicate statistically significant decreases in a one-way ANOVA with multiple hy-
964 pothesis correction. **E.** Same as in D except with the PRE mutant reporter. **F.** Images of young
965 adult hermaphrodite germlines in the *glp-1* WT 3'UTR reporter transgenic line with both DIC optics
966 (top) and GFP optics (bottom). In the DIC images, the germline is outlined in green. In the GFP
967 images, the four most proximal oocytes are bracketed in yellow. Left is treated with control RNAi,
968 right is treated with *ife-3* RNAi. **G.** Violin plot of the mean pixel intensity in the four most proximal
969 oocytes in images of germlines from the WT UTR reporter strain (green), the GBM mutant UTR
970 reporter strain (blue), and the PRE mutant UTR reporter strain (pink). The identity of the RNAi
971 target for each experiment is shown. Each dot represents an individual germline. The black bar

972 represents the median. The number of germlines imaged is shown below. The asterisks represent
973 statical significance in a one-way ANOVA with Bonferroni correction. **H**. Model for *glp-1* activation
974 by GLD-2, repression by GLD-4, and repression by IFE-3. Only repression by GLD-4 is strain-
975 specific.

976

977 **Fig. 4** CRISPR *glp-1* 3'UTR alleles made in the endogenous *glp-1(q977[glp-1::2X OLLAS*]) ge-
978 netic background [48]. The position of the GLD-1 (blue) and POS-1 (pink) binding sites are shown.
979 The blue and pink "X" marks represent the same mutations as diagrammed in figure 2C in the
980 context of the endogenous locus. The black "X" marks indicate deletion of the PAM and mutation
981 of a HindIII site to simplify screening (aagctt–aagcGt). The purple box denoted Δ71 indicates the
982 position of a 71 base pair deletion. The color of the GLP-1::2xOLLAS boxes corresponds to the
983 quantitation shown in part B and C. **B.** Violin plots representing the distribution of the total number
984 of embryos produced by a single hermaphrodite (each gray circle represents the total brood from
985 one animal). The genotype, growth temperature (20ºC and 25ºC), and the number of animals
986 assessed is shown per violin. Black bars represent the mean. The colors correspond to genotype
987 as per (A). Asterisks indicate statistical significance in a one-way ANOVA with Bonferroni correc-
988 tion for multiple hypothesis testing. **C.** Box plots of the hatch rate of the embryos produced from
989 each animal in panel (B). The individual gray circles are the hatch rate per animal, the asterisks
990 and "X" marks represent near and far Tukey outliers as in figure 2B. The total number of animals
991 assessed is listed below. The bold asterisks and gray dashed lines represent statistical signifi-
992 cance in a one-way ANOVA with Bonferroni correction. The notches and horizontal lines indicate
993 the mean.

994

995 **Fig. 5** Terminal phenotype of *glp-1(Δ71) embryos*. **A.** DIC images of early and late embryos from
996 the *glp-1(WT)*, *glp-1(Δ71)*, and *glp-1(ts)* strains. The arrows and circles identify zones of clearing
997 presumably due to apoptosis that appear to be unique to the *glp-1(Δ71)* strain. Embryonic defects
998 appear to manifest in younger embryos than in *glp-1(ts)* embryos. **B.** Stacked bar graph repre-
999 senting the percentage of normal vs. abnormal embryos observed in all three strains. The orange
1000 color reflects the fraction abnormal. Asterisks indicate statistical significance in a Chi Square test
1001 comparing each mutant to WT, with Bonferroni correction for multiple hypothesis testing.

1002

1003 **Fig. 6** Increased mitosis in the distal germline of *glp-1(Δ71)* embryos. **A.** Anti-OLLAS immuno-
1004 fluorescence, **B.** DAPI staining, and **D.** DIC images of fixed gonads from *glp-1(WT)* worms. The
1005 white dashed line in (A) indicates an example of the distance of OLLAS staining for this gonad.
1006 The white dashed line in (B) indicates the distance from the distal end to the first meiotic nucleus.
1007 **D-F.** are images collected as in (A-C) except they are of fixed gonads from *glp-1(Δ71)* worms. The
1008 white arrows in panel E indicate mitotic figures. **G.** Violin plots representing the distribution of
1009 lengths of OLLAS staining (left) or the distribution of distance from the distal tip to the first meiotic
1010 nucleus (right) for both strains. The violin plots are colored to match the strains shown in figure
1011 4A. Asterisks indicate statistical significance in a two-tailed t-test. The number of gonads analyzed
1012 is given below. **H.** Violin plots of the distribution of mitotic figures in the DAPI images in both
1013 strains. Coloring and statistical analysis are as in (G). **I.** Anti-PH-3 immunofluorescence and **J.**
1014 DIC images of fixed gonads dissected from *glp-1(WT)* animals. The white dashed bracket indi-
1015 cates PH-3 positive cells in the distal end of the germline. **K-L.** Anti-PH-3 and DIC images as in
1016 (I) and (J) except gonads were dissected from *glp-1(Δ71)* animals. **M.** Violin plot of the distribution
1017 of the number of PH-3 positive cells in both strains. Coloring and statistics are as in panel (G).

1018

1019 **Fig. 7** RNA-seq analysis of staged young adults including all strains from figure 4A. **A.** Volcano
1020 plot of *glp-1(WT)* vs. *glp-1(Δ71).* Gray circles indicate genes where the expression does not
1021 change or is not significant in a DESeq2 analysis comparing mutant to wild type expression, with
1022 a $\log_2$ fold change cut off greater than 0.585, less than -0.585, and a p_{adj} threshold of less than
1023 0.05. Increased genes are labeled in blue, and decreased genes are labeled in red. The total
1024 number of differentially expressed genes is given. **B.** Volcano plot as in (A), except *glp-1(GBM)*
1025 gene expression is compared to *glp-1(WT*)*. **C.** Same as in (B), except *glp-1(PRE)* gene expres-
1026 sion is compared to *glp-1(WT*)*. **D.** The overlap in the identity of differentially upregulated genes
1027 is compared between all three mutants in the Venn diagram. The circles are colored by genotype
1028 as in figure 4A. **E.** A Venn diagram as in (D), except downregulated genes are compared. **F.**
1029 Wormcat 2.0 analysis of the total regulated gene set in *glp-1(Δ71)* vs. *glp-1(WT)*. Category 1 (non-
1030 italics) and 2 (italics) changes are grouped by pathway. The size of the circle indicates the counts
1031 of genes in each category, and the color represents the P-value from the Wormcat 2.0 analysis.

1032 **TABLE 1:** Strains used in this study

Strain ID	Genotype	Approach	Reference
N2	WT	N/A	[68]
WRM5	*sprSi5[Pmex-5::MODC PEST:GFP:H2B::glp-1 3'UTR cb-unc-119(+)]* II, *unc-119(ed3)* III	mosSCI	[32]
WRM6	*sprSi6[Pmex-5::MODC PEST:GFP:H2B::glp-1 3'UTR(ΔGBM) cb-unc-119(+)]* II, *unc-119(ed3)* III	mosSCI	[32]
WRM9	*sprSi9[Pmex-5::MODC PEST:GFP:H2B::glp-1 3'UTR(Δ5'3' PRE) cb-unc-119(+)]* II, *unc-119(ed3)* III	mosSCI	[32]
JK5973	*glp-1(q997[glp-1::2xOLLAS])* III	CRISPR	[48]
WRM73	*glp-1(spr16[q997*(glp-1::2XOL-LAS::Δ71_3'UTR])* III	CRISPR	This paper
WRM83	*glp-1(spr21[q997*(glp-1::2XOL-LAS::WT_3'UTR (HindIII site)]* III	CRISPR	This paper
WRM84	*glp-1(spr22[q997*(glp-1::2XOLLAS:: 5'3'PRE _3'UTR (HindIII site)]* III	CRISPR	This paper
WRM109	*glp-1(spr33[q997*(glp-1::2XOL-LAS::GBM_3'UTR (HindIII site)]* III	CRISPR	This paper
EU552	*glp-1(or178)* III	EMS	Un-published

1033

1034 **SUPPLEMENTAL INFORMATION**

1035 1. Supplemental Table 1: Primers and oligonucleotides
1036 2. Supplemental Data Set 1: Numerical data and statistical tests (.xlsx)
1037 3. Supplemental Data Set 2: RNA sequencing analysis output files (.tar.gz)
1038 4. Supplemental Data Set 3: Scripts and output for PAT-seq analyses (.tar.gz)
1039

1040 **Supplemental Table 1** *Primers and oligonucleotides used in this study*

Name	Sequence (5' to 3')	Purpose
ife-1F	5'-TAATACGACTCACTATAGGGGTCAGATTCTGAAATAGCATTT-GAGAAGC-3'	RNAi
ife-1R	5'-TAATACGACTCACTATAGGGGACGGCGGATTTCTCGGC-3'	RNAi
ife-2F	5'-TAATACGACTCACTATAGGGGTCCGAAGAACCAGTCGCAG-3'	RNAi
ife-2R	5'-TAATACGACTCACTATAGGGTAAGTGGCTGGTGTGGCAGG-3'	RNAi
ife-3F	5'-TAATACGACTCACTATAGGGGAGGATTGTCTGAA-GATGGTTTCACTTTTCG-3'	RNAi
ife-3R	5'-TAATACGACTCACTATAGGGGAGATCTTTAGAA-TATGCTTAAGGAGTTGGGG-3'	RNAi
F21	5'-CGGTCAATGCGATGTGGTAT-3'	PCR
R21	5'-GAGCCTCGAGAATGGTGAGT-3'	PCR
C10T2	5'-CCCCCCCCCCTT-3'	CDNA
M13RC 0T2 for tail	5'-CAGGAAACAGCTATGACCCCCCCCCCCTT-3'	PCR
FP	5'-GCGATGGCCCTGTCCTTTTA-3'	PCR
RP for gene	5'-GGGACCAGTGTCTGGGTGATGT-3'	PCR

gld-2F	5'-AGTACGGCCGTTGGTATCAG-3'	RNAi
gld-2R	5'-ATGTTGCTGCTGATTGTTGC-3'	RNAi
gld-4F	5'-TTTCGGAGCGAGAAGACACT-3'	RNAi
gld-4R	5'-GTGGCTGAGTTGTTGTCGAA-3'	RNAi
crRNA	5'-CTTATACTCTTAATCTGATT-3'	CRISPR
Repair DNA Oligo Δ71	5'- CAGACACTGGTCCCCACAGAGTTTTTTGTATACTACAGAT-TAAGAGTATAAGCTTTGTTTTTTCTCCTTT-3'	CRISPR
ssODN WT*	5'-TATTGTAAGCTATAAGTTGTAGAATAATTATTGATAATCAGAT-TAAGAGTATAAGCGTT-GTTTTTTCTCCTTTTCTTTATAACTTGTTACAA-3'	CRISPR
ssODN GBM	5'-GTATACTATTTCGGGTCATTTTTCTTATTCTAGACCAA-TATTGTAAGCTATAAGTTGTAGAA-TAATTATTGATAATCAGATTAAGAGTATAAGCGTTGTTTTTTCTCCTTTTCTTTATAACTTGTTACAA-3'	CRISPR
ssODN 5'3'PRE	5'-AGAGTTTTTTGTATACTATTTCGGGTCATTTTTCTCCCTCTA-GACTAACCCTGTAAGC-TATAAGTTGTAGAATAATTATTGATAATCAGATTAAGAGTATAAGCGTTGTTTTTTCTCCTTTTCTTTATAACTTGTTACAA-3'	CRISPR

1041

1042

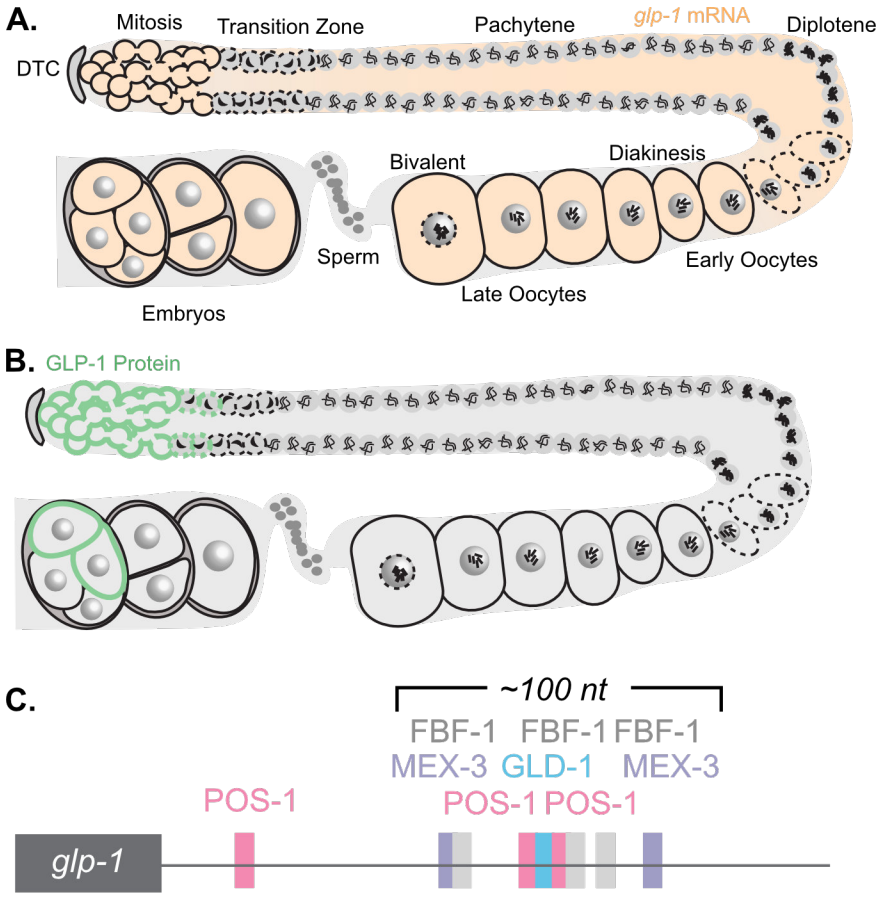

Figure 1
Coskun and Ryder, 2026

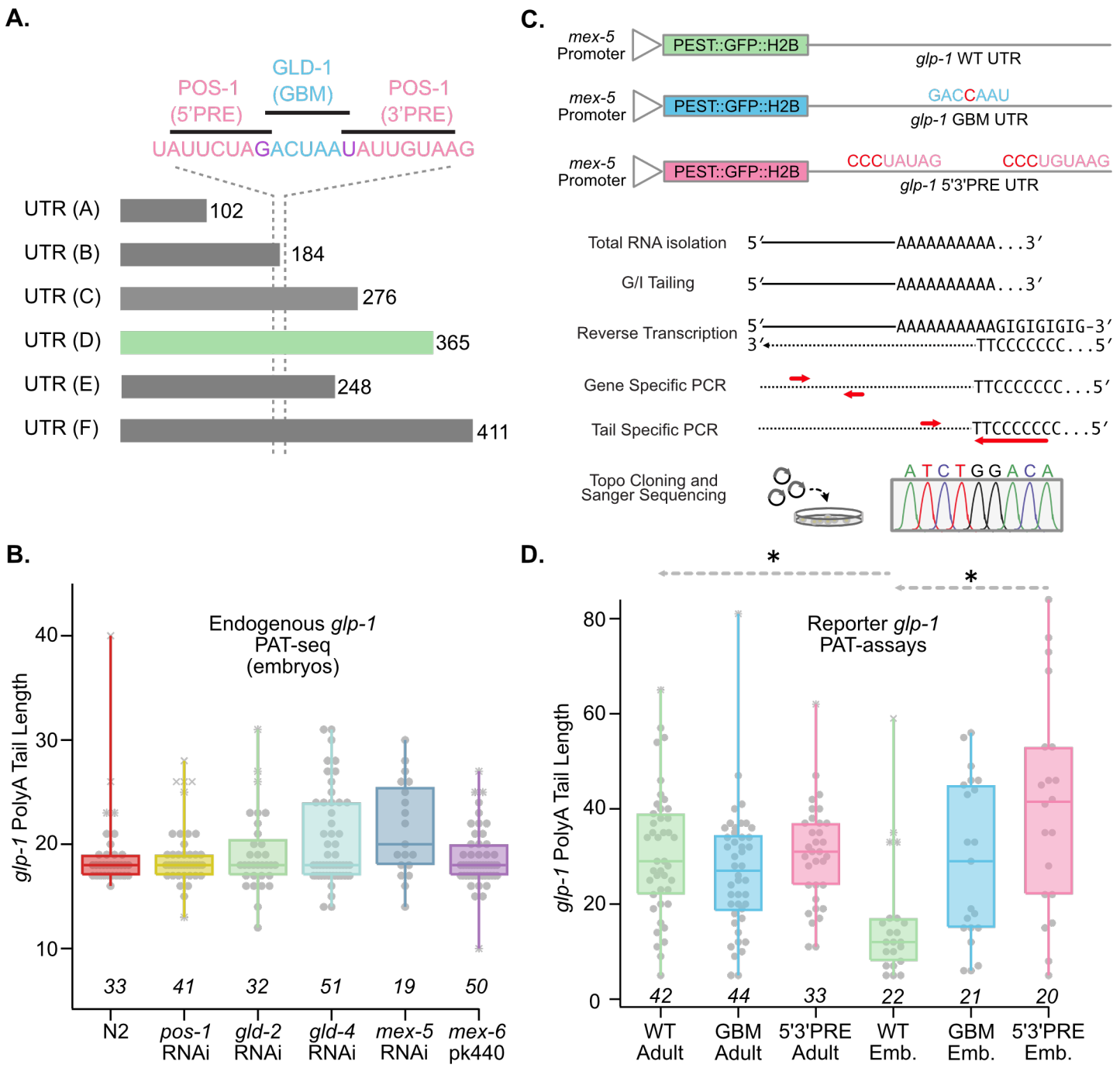

Figure 2
Coskun and Ryder, 2026

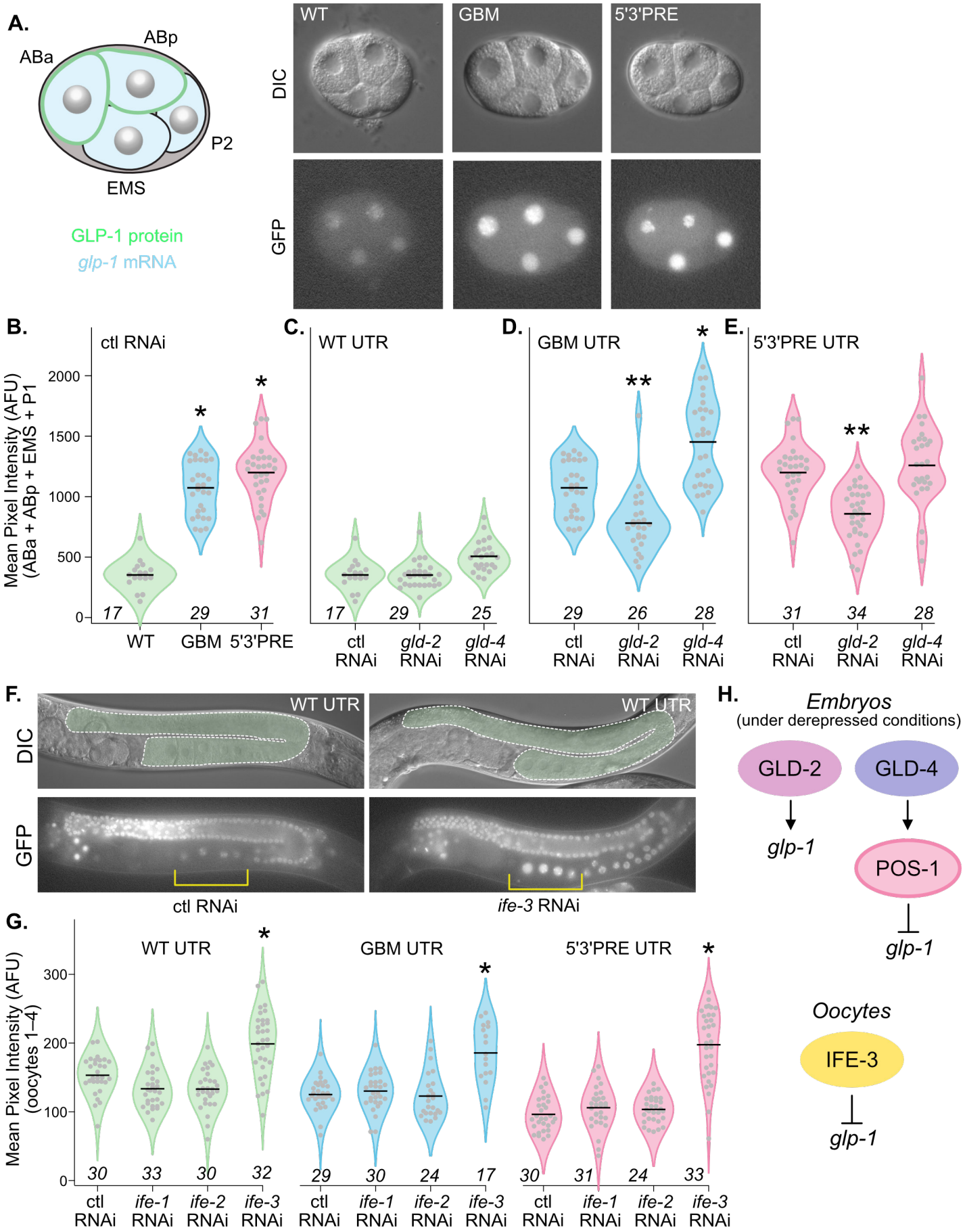

Figure 3
Coskun and Ryder, 2026

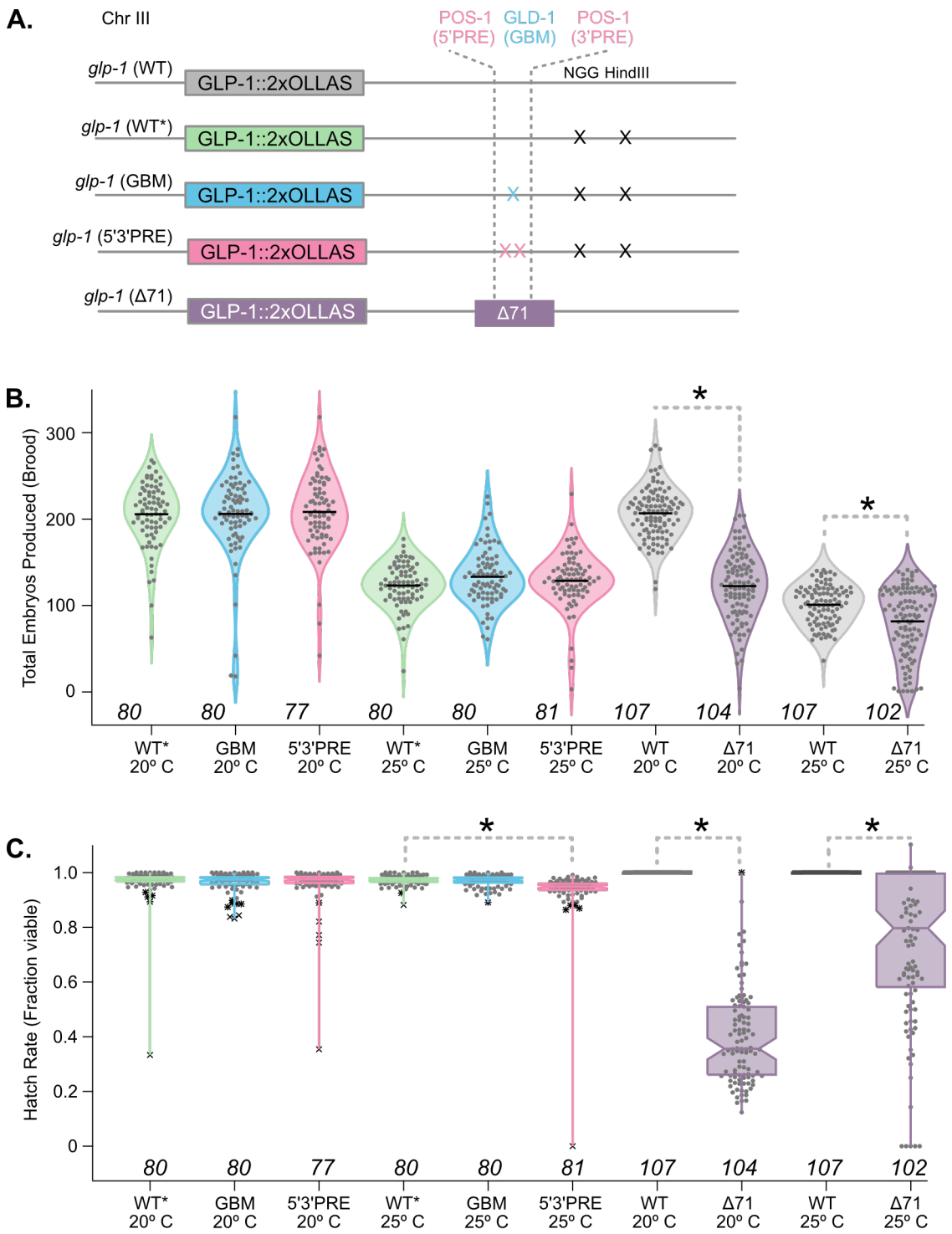

Figure 4
Coskun and Ryder, 2026

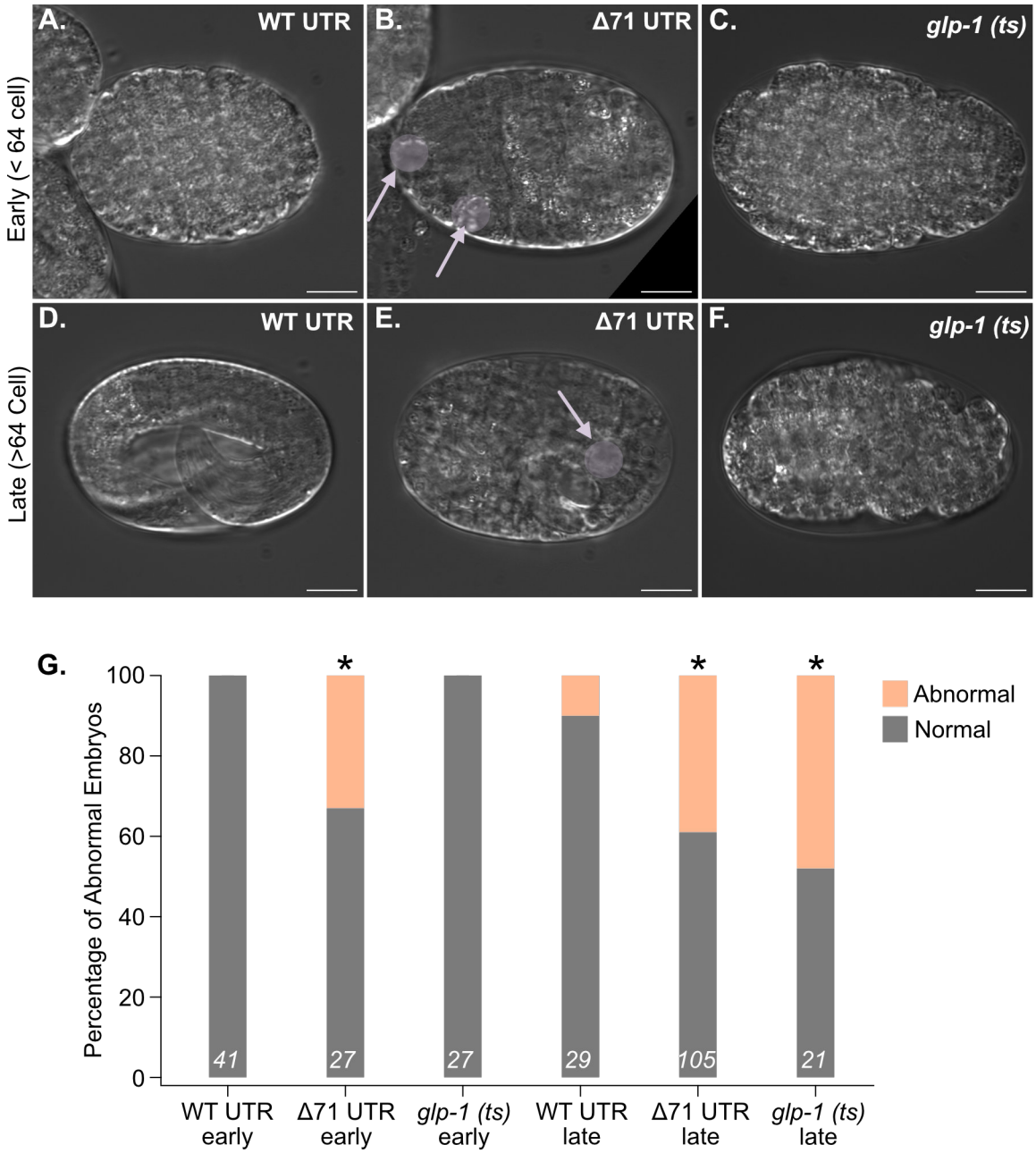

Figure 5
Coskun and Ryder, 2026

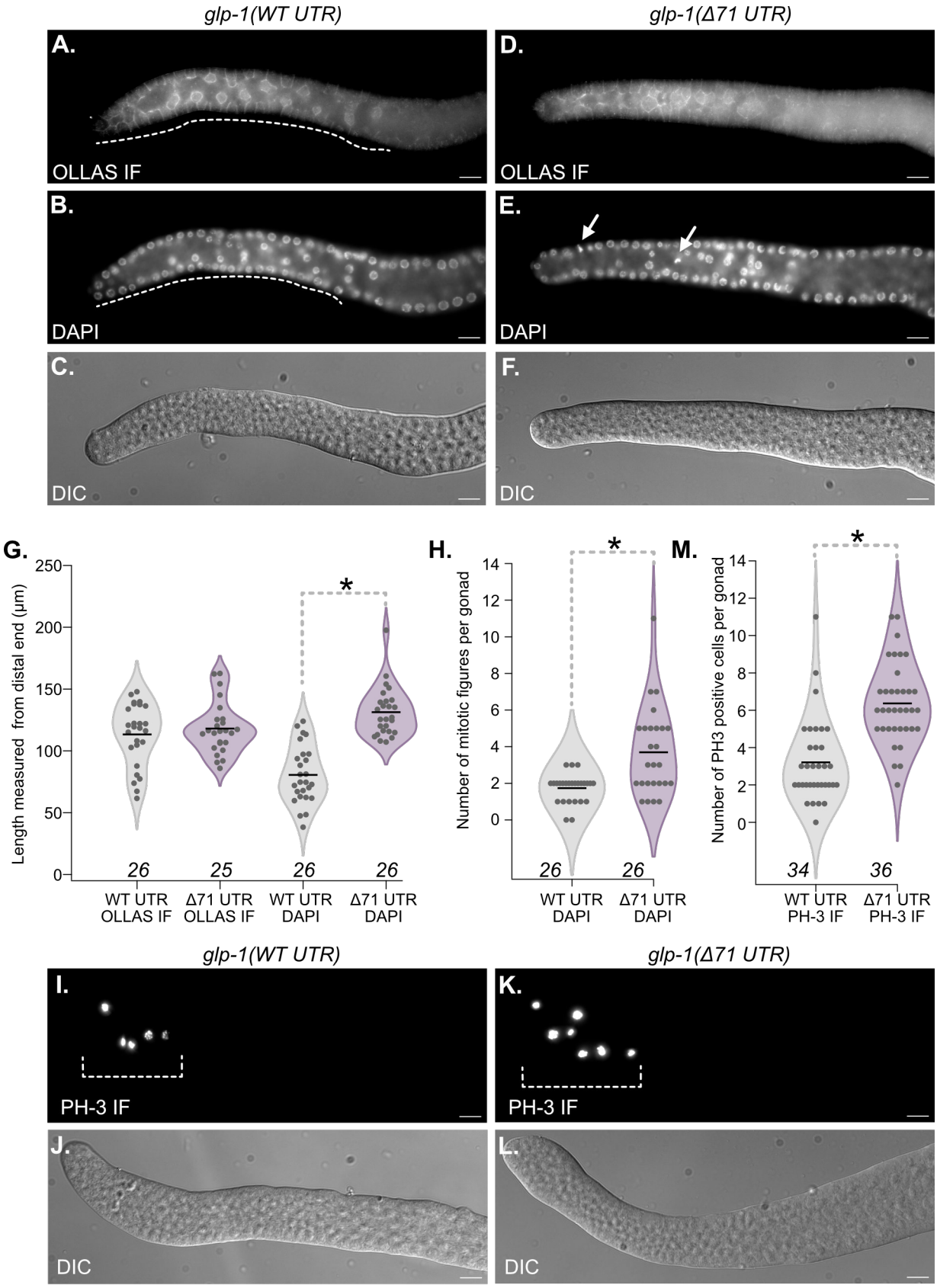

Figure 6
Coskun and Ryder, 2026

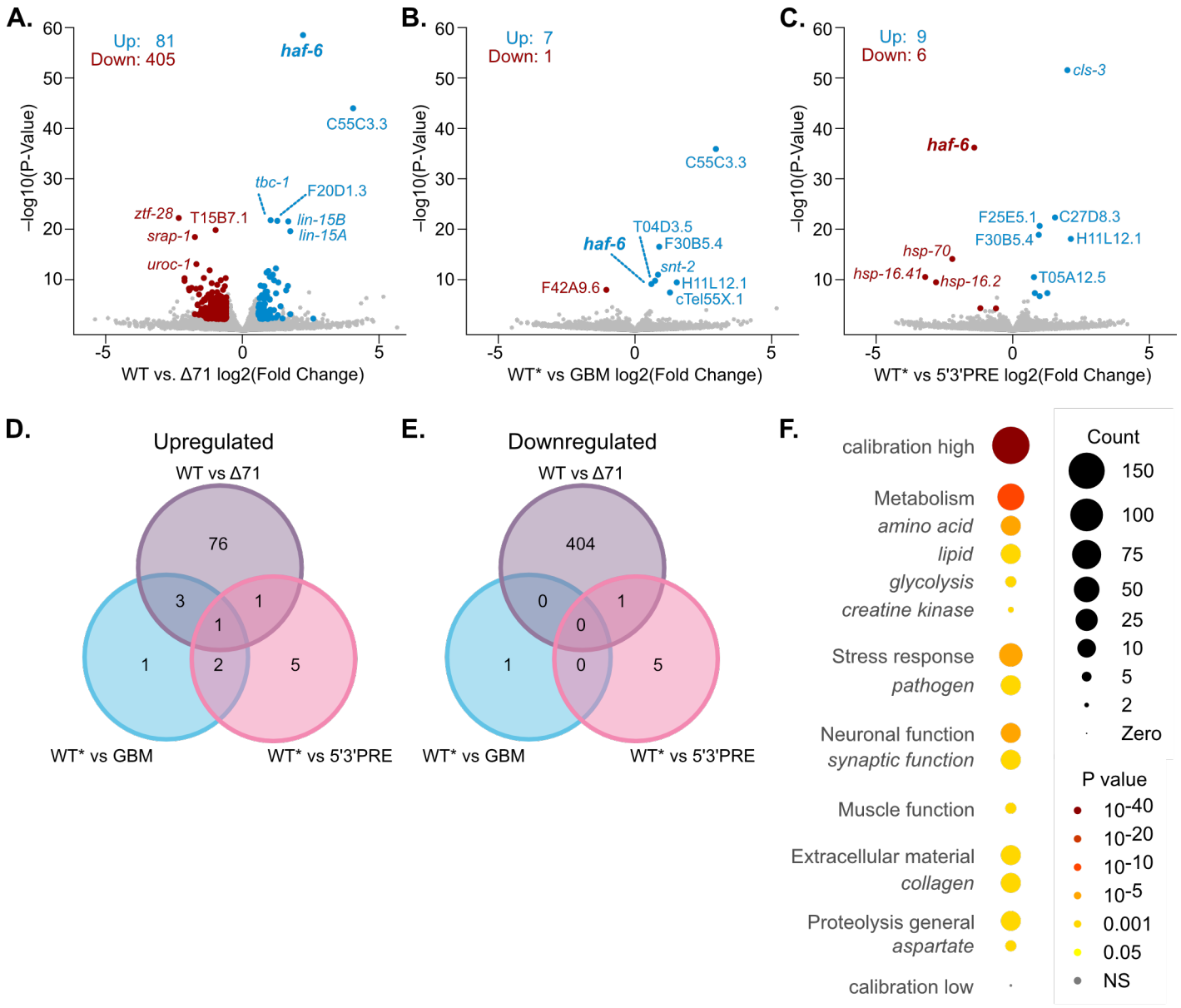

Figure 7
Coskun and Ryder, 2026